Excitonic processes and lasing in ZnO thin films and micro/nanostructures

Aika Tashiro,[1] Yutaka Adachi[2] and Takashi Uchino[1,a)]

[1]*Department of Chemistry, Graduate School of Science, Kobe University, Nada, Kobe 657-8501, Japan*

[2]*Optoelectronic Materials Group, Optical and Electronic Materials Unit, National Institute for Materials Science, Tsukuba, Ibaraki 305-0044, Japan*

[a)] Author to whom correspondence should be addressed: uchino@kobe-u.ac.jp

Low dimensional ZnO-based materials have drawn much attention for the past decades due to their unique electronic and optical properties and potential applications in optoelectronic devices. In this tutorial, we will cover the past and the latest developments in ZnO thin films and micro/nanostructures in terms of excitonic and related lasing processes. First, we will give a brief overview of temperature-dependent linear excitonic absorption and luminescence spectra. Second, we will introduce feedback mechanism for lasing in various forms of ZnO, ranging from nanoparticles to nanowires, nanodisks and

thin films. As for the feedback mechanism, detailed descriptions are given to random lasing, Fabry-Perót lasing, and whispering gallery mode lasing. Third, we discuss possible gain mechanisms, i.e., excitonic gain and electron-hole plasma (EHP) gain, in ZnO. A special interest is also devoted to the Mott carrier density, which is a crucial parameter to distinguish between excitonic and EHP contributions to lasing.

I. INTRODUCTION

Since the middle of the last century, ZnO began to attract interest for its interesting optical and electronic properties, such as a wide direct bad gap of 3.37 eV at room temperature and the native n-type conductivity.[1,2] In the early stage of the research, optical absorption, reflection, and emission characteristics have been extensively investigated using high-quality ZnO single crystals. It was revealed that ZnO exhibits various non-linear phenomena under high electronic excitation, resulting in excitonic and electron-hole plasma (EHP) stimulated recombination processes, especially at cryogenic temperatures, as will be shown in detail in later sections. In addition, its relatively high exciton binding energy E_X^b ($E_X^b = 60$ meV)[3,4] allows us to anticipate the possibility of excitonic stimulated emission and lasing even at room temperature.

In the late 1990s and early 2000s, the progress of nanofabrication technologies enables the formation of a variety of ZnO-related micro/nanostructures, including epitaxial layers,[5–8] nanoparticles,[9] nanowires,[10] and quantum wells,[11] which allows us to observe room-temperature lasing with a narrow spectrum. Accordingly, ZnO has attracted renewed and growing interest from the scientific community, leading to remarkable recent progress in the field of nanowire photonics,[12–14] disordered photonics[15–17] and polaritonic devices.[18–21]

The purpose of this Tutorial is to provide an overview of these past and upcoming fields such that readers may get a glimpse of the landscape of the excitonic processes and the related high-excitation phenomena including excitonic and EHP lasing in ZnO thin films and micro/nanostructures. The rest of the article is organized as follows. Section II reviews the basic optical and excitonic properties. Sections III and IV discuss the feedback and gain mechanisms for lasing, respectively. Conclusions are given in Sec. V. This Tutorial is by no means a comprehensive review on the structural, optical and emission properties of ZnO micro/nanostructures, for which the readers are referred to existing and recent review articles.[1,22–29]

II. BASIC OPTICAL AND EXCITONIC PROPERTIES

Optical and excitonic properties in ZnO have been investigated by various techniques, such as optical absorption,[30] reflection[3,4,31,32] photoluminescence[4,33,34] and cathodoluminescence spectroscopies.[35,36] In this section, we will focus solely on optical absorption and photoluminescence properties, both of which are especially useful to characterize the band gap and related optical properties of semiconductors.

A. Optical absorption

Measuring the optical absorption is the most simple but direct method for probing the band structure of semiconductors. Since ZnO is a direct band gap semiconductor, the spectral dependence of the fundamental absorption coefficient α can be described as follows:[37]

$$\alpha h\nu = A(h\nu - E_g)^{1/2} \quad , \qquad (1)$$

where h is Planck's constant, ν is the photon's frequency, E_g is the band gap energy, and A is a proportionality constant. According to Eq. (1), E_g can be evaluated by plotting $(\alpha h\nu)^2$ versus $h\nu$, which is called the Tauc plot. Although the Tauc plot is frequently used to evaluate the optical band gap of ZnO and ZnO-based materials,[38–40]

this method does not yield the correct band-gap values because of the predominance of a free exciton absorption just below the fundamental gap.[1] Thus, the E_g value obtained by this method has a significant uncertainty especially at low temperatures.[41]

From these arguments, it is useful and necessary to know how the free exciton absorption affects the shape of the fundamental absorption edge of ZnO depending on the measurement temperature. However, reports on the temperature dependence of the optical absorption spectra of ZnO are rather limited,[30,41–43] and no systematic temperature-dependent behavior of the excitonic absorptions has been published yet. Thus, in this tutorial, we measured the temperature-dependent (5-300 K) optical absorption spectra of a ZnO thin film with thickness *d* of 249 nm, which was grown by a pulsed laser deposition (PLD) method (for details see the supplemental material), as shown in Fig. 1(a). The absorption spectrum measured at 5 K shows three major peaks at 3.371, 3.444 and 3.52 eV [see the inset of Fig. 1(a)], in good agreement with those reported previously on single-crystal ZnO thin platelets grown by the vapor transport method.[30] One sees that the peak at 3.371 eV is not symmetric, which is most likely due to the overlap of the A and B free excitons.[22,30] The other high-energy peaks at 3.444 and 3.52 eV are attributed to exciton-one-phonon and exciton-two-phonon complexes, respectively,[30] although the C free exciton may also contribute to the lower energy side of the 3.444-eV peak.[22,30] The

appearance of the exciton-phonon complexes will ensure the high quality of the present PLD grown film. Since the excitonic absorptions are clearly identified in the low-temperature absorption measurement, the temperature dependent change in the peak energy yields information about the temperature dependence of the band gap energy, which is located above the A exciton peak by E_X^b = 60 meV. Although similar information can be obtained from the temperature-dependent reflectance[31] and photoluminescence[4,33] spectra, the advantage of the optical absorption technique over the other methods is that the output data are directly used to identify the position of the free exciton peaks. In the present absorption spectra, the positions of the A and B excitons are not clearly resolved, as noted earlier. However, it can safely be assumed that the peak position of the 3.371-eV peak observed at 5 K represents that of the A exciton of our sample as this value is in reasonable agreement, within our spectral resolution (~0.005 eV), with those reported previously for the free A-exciton in ZnO single crystals ($\mathrm{FX}_A^{n=1}$ = 3.3768–3.3781 eV).[3,4,30,44] Figure 1(b) shows the temperature-dependent variation of the A-exciton peak energy shown in Fig. 1(a). Although several equations have been proposed to represent the temperature dependence of the bandgap (E_g) and free-exciton ($E_{\mathrm{FX}} = E_g - E_X^b$) energies in semiconductors,[45,46] we found that the observed temperature dependence can be best fitted to Bose-Einstein model,[47]

$$E_{\mathrm{FX}}(T) = E_{\mathrm{FX}}(0) - \frac{k}{\exp\left(\frac{\theta}{T}\right) - 1} \ , \qquad (2)$$

where k is a constant and θ is the parameter related to the average phonon frequency or the Einstein characteristic temperature. The fitted values of θ and k in Eq. (2) are 349.4 K and 0.118, respectively, which are comparable to those obtained by photoluminescence[31] (θ = 380 K and k=0.177) and photoluminescence excitation[48] (240 K and k=0.09) measurements. From these fitted parameters in Eq. (2) and E_X^b= 60 meV, we can estimate the temperature dependence of the band gap $E_g(T)$, as shown in the red solid curve in Fig. 1(b). This estimation yields the band gap of 3.377 eV at 300 K, in reasonable agreement with the mostly accepted band gap of ~3.37 eV at room temperature.[22] This allows us to confirm that the measurement of optical absorption spectra is useful and effective to obtain the temperature dependence of the band gap in ZnO.

B. Photoluminescence

Photoluminescence (PL) of ZnO is very rich in structure and depend strongly on the size, shape, crystallinity, impurity and surface states of the sample of interest. Although

its surface sensitive nature often complicates the interpretation of the resulting PL spectra, it can become a powerful method to assess surface phenomena and can be exploited for sensing applications, e.g., PL-based biosensors.[49,50]

The PL emissions of ZnO are usually categorized into two energy regimes: near band edge (NBE) ultraviolet (UV) and deep level visible emissions. In the NBE UV spectral region, ZnO single crystals exhibit a number of emission lines, when probed at low temperatures, due not only to free exciton (FX) states but also to bond-exciton states, two electron satellite transitions of shallow bound excitons, and donor-acceptor-pair recombinations (Fig. 2).[4,22,51–53] As for ZnO nanostructures, one also finds emissions of surface excitons (SX)[54–56] along with the controversial PL peak at 3.31eV (Fig. 3, for details see Refs.[57–61]) Respective UV emission peaks are often accompanied by longitudinal optical (LO) phonon replicas with an energy separation of ~72 meV[57–62] (Figs. 3 and 4).

In general, the PL of the donor-bound excitons is the most intense PL band for temperatures $T < \sim 10$ K, while the PL of the FX tends to dominate the spectrum at higher ($T > \sim 200$ K) temperatures[4,22,61,62] (Figs. 3 and 4). These temperature dependent changes in the PL spectra result from thermal activation of the donor-bound excitons into excited states where they behave as free excitons. Accordingly, at room temperature one finds

one broad PL band due to the line broadening of the FX peak and its *n*LO-phonon (*n* = 1, 2...) replicas.[63] Typically at room temperature, the NBE UV peak of ZnO films and nanostructures is located in the energy range from 3.15 to 3.30 eV,[23,61,62,64–70] whereas the bulk ZnO single crystal shows NBE PL emission peaking at 3.30-3.31 eV.[1,25,63–69] These NBE PL energies are slightly lower than the free exciton absorption energy from the absorption measurement of ZnO at 295 K (3.32 eV),[30] as also shown in Fig. 1. This confirms that at room temperature, the spectral shape of the FX PL band is substantially affected by the presence of LO phonon replicas[1] and/or the effect of reabsorption.[1,25]

The defect and impurity states in ZnO yield deep level emission bands in the visible spectral region, showing blue, green, yellow and orange/red PL bands.[22,23] There have been a huge number of studies on the emission properties of these deep level PL bands, which are still a matter of intensive research.[72–79] It should be noted, however, that the existence of deep-level emissions does not have a significant effect on the stimulated emission since the ratio of the visible emission to the NBE emission decreases as the excitation density increases.[67,80] Thus, we do not give details here; the interested reader should consult referenecs[22,23,34,50] for a review on the deep level emissions in ZnO.

III. FEEDBACK MECHANISM FOR LASING

The laser has had a tremendous impact on many different areas of science, including physics, chemistry, astronomy, biology and medicine. Since the first demonstration of the laser in 1960, great progress in improving the extent of the spatial and temporal coherence of laser light has been made and still research is ongoing especially in terms of the lasers with complex light patterns.[81–84] In general, three core elements are necessary for making a laser; that is, gain medium, a means to excite it, and an optical resonator for optical feedback. In ZnO-based laser, ZnO itself behaves both as a gain medium and a resonator. It should be noted that its dimension and size are highly versatile, including nanoparticle, nanowire, nanoribon, and thin film. Accordingly, two principal feedback mechanisms, i.e., random lasing and microcavity lasing, are observed depending on its morphologies.

A. Random lasing

As mentioned above, an optical resonator is one important element in achieving laser action. An optical resonator or cavity is a system in which light at certain frequencies is continuously reflected back and forth without escaping, building up power in the process.[85] For this purpose, a two-mirror cavity is conventionally employed [Fig. 5(a)]. In random lasers, however, a completely different feedback mechanism, i.e., multiple scattering, is used to realize optical feedback [Fig. 5(b)]. Thus, random lasers, along with

recently emerged plasmon lasers[86] and topological lasers,[87,88] have considered as a paradigmatic phenomenon of laser systems, opening up a new perspective in the photonics in disordered media.[82,89–94] During the last several decades, random lasing action has been demonstrated in a variety of random media, as described in recent review articles.[95–98] Among other experiments on random lasers, the results reported by the group of Cao *et al.* on ZnO polycrystalline films[99] and nanoparticles[9,100] are worth mentioning, in that they first observed the narrow and intense lasing peaks with the linewidth less than 0.3 nm under pulsed laser pumping (Fig. 6). These phenomena give evidence for the light amplification through a coherent feedback of the interference effects, hence stimulating further investigations into random lasers and related disordered photonics[16,101] in terms of mode localization and interaction,[102–104] mode-locking,[105,106] and controlling directionality.[107]

In discussing the nature of light scattering in a three-dimensional (3D) system, it is useful to define the following length scales (Fig. 7):[89]

scattering mean free path (l_s) – an average distance that photons travel between two successive scattering events.

transport mean free path (l_t) – an average distance over which the direction of propagation of waves is randomized by scattering.

gain length (l_g) – a distance over which the intensity optical signal is amplified by a factor $e \approx 2.72$ in a gain medium without scattering.

amplification length (l_a) – a root mean square distance between the beginning and ending point for paths of length l_g in a gain medium with scattering. In the limit without scattering, $l_a = l_g$. In the presence of scattering, l_a becomes shorter than l_g, leading to higher effective gain coefficient.

The above lengths scales are related to each other as follows:

$$l_t = \frac{l_s}{1 - \langle \cos\theta \rangle} \ , \qquad (3)$$

$$l_a = \sqrt{\frac{l_t l_g}{3}} \ , \qquad (4)$$

where $\langle \cos\theta \rangle$ is the average cosine of the scattering angle. Depending on the relative magnitude of these characteristic length scales, scattering phenomena of light with wavelength λ in 3D medium with size L can be classified into three regimes: (i) the ballistic regime, $L < l_t$, (ii) the diffusive regime, $\lambda < l_t < L$, and the localization regime, $l_s < \lambda$. Practically, light scattering in the diffusive and localization regimes is a main concern for both experimentalists and theorists.

1. Localization regime

In the localization regime, strong phonon localization in confined space can be realized. This is analogue to the electronic Anderson localization,[108] which is a theoretical basis for the metal-insulator transition in condensed matter systems. Although Anderson-like light localization was once recognized as one potential mechanism for the narrow laser spikes observed in random laser systems, no such light localization in the sense of an Anderson localization has been realized in ZnO nanoparticle-based random lasers, as will be shown in the next subsection. Generally, Anderson-like light localization requires a special design of scattering media, such as 2D[109] or 3D[110] photonic crystals, a disordered photonic-crystal waveguide,[111] a planar nanophotonic network,[112] and a randomly spaced air-grooves,[113] to satisfy the condition $l_s < \lambda$.

2. Diffusive regime

As noted earlier, random lasing spikes were first observed in ZnO polycrystalline films[99] and nanoparticles[9,100] with particles sizes of 50–150 nm (Fig. 6). The demonstration of the sharp lasing spikes indicates that the observed lasing behavior arises from resonant (coherent) feedback.[15,89] These ZnO nanoaggregates are especially suitable

for resonant feedback due to their relatively high refractive index n ($n \approx 2.3$ in the near band edge region), providing efficient scattering for coherent random lasing. In addition to ZnO nanoparticle, ZnO nanoneedle arrays (the diameter of the stem part is ~100nm) grown perpendicular to a planar substrate have been shown to demonstrate sharp lasing spikes due to in-plane light scattering (Fig. 8).[114] It should be noted that in closely packed monodisperse ZnO powders with size d of ~140 nm, the transport mean free path l_t is estimated to be 1.2 μm for λ = 400 nm.[115] When d decreased, l_t further increased. Thus, the light scattering responsible for the random lasing spikes in the ZnO particles will not occur in the localized regime ($l_s < \lambda$) but in the diffusive regime ($\lambda < l_t < L$). In the diffusive regime, the optical modes are expected to be broad and overlap spectrally and spatially. The resulting feedback would be nonresonant, and hence the emission spectrum will narrow continuously towards the center of the gain spectra with increasing pumping intensity,[89,91] resulting in the amplified spontaneous emission (ASE). ASE is a light emission process in which spontaneously emitted photons are amplified by stimulated emission as they travel through a gain medium without coherent feedback.[116] Such incoherent random lasing was indeed observed in powders of laser crystals including $NdAl_3(BO_3)_4$, $NdSc_3(BO_3)_4$, and $Nd:Sr_5(PO_4)_3F$ (ref. 117) and colored LiF (ref. 118) and MgO (refs. 119–121) crystals. Therefore, it has been an open question as to why narrow

coherent lasing spikes are observed in such diffusive systems. Two different scenarios have been proposed for the origin. One is a model based on the formation of ring-shaped resonators with index of refraction larger than average, leading to local cavities (local modes).[122,123] Another is a model based on the formation of open modes where spontaneously emitted photons accumulate gain along very long trajectories.[114,115] The resulting "lucky photons" accumulate enough gain to activate a new lasing mode with a different wavelength after each excitation shot, giving rise to random spikes in the emission spectrum. Later, it has been found from a full solution of Maxwell's equations including a polarization term due to the atomic population inversion that even in the diffusive and weak scattering regimes, modes expand over the whole sample and overlap both spatially and spectrally (Fig. 9), leading to resonant feedback with spectrally narrow emission.[126,127] It is hence of interest to investigate which mode, local or open mode, is responsible for the lasing spikes observed in diffusive random systems. The answer to this question is not straightforward and will dependent strongly on the experimental system. As far as the ZnO nanoparticle powders are concerned, Fellert and co-workers[128] have demonstrated that strongly localized random lasing modes co-exist with modes of much larger spatial extension (Fig. 10). They[128] have shown that the extended modes are primarily found in the spectral region where the gain is expected to be highest, whereas

the strongly localized modes are found in regions where the available gains is lower. This observation is consistent with the prediction that localized modes have a lower loss rate than that of extended modes.[16] Hence, it is most likely that both extended and localized modes in diffusive random systems can contribute to the occurrence of narrow lasing spikes. The relative dominance of these two modes will be governed by the spatial distribution of gain and loss in the random system of interest.

B. Microcavity lasing

One of the biggest advantages of ZnO is that it can be grown in a shape of optical cavity, including nanorods, nanowires, nanoribbons, nanocombs, nanosawsand nanotetrapods and so forth.[129–131] These intriguing ZnO micro/nanostructures can be prepared by both gas-phase[132–136] and solution-phase[137–142] methods. Among other techniques, the vapor-liquid-solid (VLS) growth method has achieved the most success in producing optical cavities in relatively large quantities (Fig. 11).[132–134] As for microcavity lasing, 1D microrod and 2D microdisk structures are of particular interest.[12,62,143,144] In microcavity lasers, the micro/nanostructure itself act both as a optical cavity and a gain medium, providing an ideal experimental platform for the development of miniature-cavity-based optoelectronic devices.[145–147] Depending on the

resonant cavity structures, microcavity lasing can be classified into two groups. The first is Fabry-Perót (F-P) lasing observed in nanorods [Fig. 12(a)] with diameters and lengths of ~50–~500 nm and ~1–~100 μm, respectively, where light is amplified along the two end planes of the nanorod perpendicular to the nanorod axis.[13,148,149] The second is whispering gallery mode (WGM) lasing [Fig. 12(b)] observed in ZnO nanorods and nanodisks with cross-sectional diameters greater than ~1 μm,[150–155] where light propagates circularly in the cavity due to the multiple total reflection at the inner walls of ZnO cross-section..

1. *Fabry-Perót (F-P) lasing*

In 2001, Huang *et al.*[10] reported a room-temperature optically pumped laser from ZnO single-crystalline nanowire arrays. This is the first experimental demonstration of nanowire lasers without any fabricated mirror. The advantage of FP microlasers is that by designing the compositional, geometrical and structural parameters of the nanostructures, it is possible to control the lasing characteristics, for example, *Q* factor, lasing threshold, number of modes, and lasing wavelengths. Lasing characteristics of a single ZnO nanowire was also subsequently reported (Fig. 13).[156,157]

In the nanowire cavity, lasing occurs when the round-trip gain compensates the total cavity losses,[146]

$$\Gamma g_{th} > \alpha_m + a_p = \frac{1}{2L}\ln\left(\frac{1}{R_1 R_2}\right) + a_p, \qquad (5)$$

where Γ is the confinement factor, g_{th} is the threshold gain, α_m is the mirror loss, α_p is the propagation loss, and R_i (i=1,2) is the effective reflectivity at the ZnO/air boundary of the two end-facets (R≈15.5 %). Γg_{th} is commonly referred to as the modal gain, meaning that the percentage power increase per unit length along the propagation direction gained by the waveguide mode from the active region.[149] In nanowire lasers, α_m is much larger than a_p due to the smaller cavity length and the smaller reflection coefficient. Hence, it follows that Γg_{th} as well as Q factor is strongly dependent both on L and the nanowire diameter D as R is a strong function not only of the mode type and lasing frequency but also of D.[149,158] The exact determination of the modal gain is quite challenging for microcavities. Richters *et al.*[159] determined experimentally the modal gain of single-ZnO nano- and microwires using the variable-stripe-length method (VLS) and found that it reaches a maximum value of 5000 cm^{-1} with increasing D up to 1.2 μm (Fig. 14). For the experimental details of the VLS technique, see references.[160,161]

The Q factor and the spacing $\Delta\lambda$ between individual laser modes for a F-P cavity are described respectively by[157,162]

$$Q = \frac{2\pi nL}{\lambda(1-\sqrt{R_1R_2})}, \qquad (6)$$

$$\Delta\lambda = \frac{\lambda^2}{2L\left(n-\lambda\frac{dn}{d\lambda}\right)}, \qquad (7)$$

where n is the refractive index, L is the cavity length which is equal to the distance between the two opposite side surfaces of the nanowire, and λ is the lasing wavelength. The Q factor obtained from Eq. (6) is an ideal upper limit value provided that the optical absorption and scattering inside the cavity are neglected. For a nanowire with length of 10 μm, Eq. (6) yields the Q factor of ~500 at λ =350 nm. This estimated Q factor is in reasonable agreement with the observed Q factor obtained from the full width at the half maximum δλ (FWHM) of the lasing spike peaking at λ (Q=λ/δλ) in high-quality ZnO nanowires.[62] Since the report on the ZnO nanowire lasers, optically excited laser action has been demonstrated for a variety of ZnO micro/nanostructures, such as nanoribons,[163] nanobelts,[164] and tetrapods.[165] In ZnO nanoribbons, pseudo-rectangular cross-sections lead to excellent microcavities with a high Q factor of ~3000.[163]

Figure 15 shows a representative x-ray diffraction (XRD) pattern of a ZnO nanowire ensemble sample prepared by a VLS growth method along with its scanning electron microscope (SEM) and bright-field and high-resolution transmission electron microscope (HRTEM) images,[149,166] illustrating an excellent crystallinity of an individual nanowire (L = 100 μm, D =100-400 nm). Figure 16 shows the pump-intensity-dependent PL spectra of these ZnO nanowires under excitation with the third harmonic (355 nm) of a nanosecond pulsed Nd:YAG laser. For pump intensity I_{ex} ≤200 kW cm^{-2}, the spectra are broad and featureless, centered around 382 nm and with FWHM of 19.3 nm. In this regime, light is emitted essentially isotropically along the nanowire [Fig. 16(b)], and the output power depends linearly on the excitation intensity [Fig. 16(c)], showing the occurrence of spontaneous emission. In the pump intensity region from 200 kWcm^{-2} to 300 kWcm^{-2}, the spectra consist of a broad emission with the addition of sharp FWHM 0.4 nm emission lines. In this regime, population inversion starts building up, leading to

ASE along the nanowire at wavelengths corresponding to the enhanced emission from the nanowire ends [Fig. 16(b)]. Furthermore, the output power exhibits a superlinear increase with pump intensity [Fig. 16(d)], which is the expected behavior as the laser threshold is approached.[167] For $I_{ex} > 300$ kW cm^{-2}, the spectra are dominated by sharp emission lines with intensity that is orders of magnitude greater than the spontaneous emission background [Fig. 16(a)]. Thus, in general, the threshold in semiconductor lasers is "softer" than that in other lasers due to the small cavity volume and to the relatively high levels of spontaneous emission.[167]

Recently, it has been shown that through the coupling between metal surface plasmon modes and FP modes of ZnO, surface plasmonic lasers are realized.[168,169] In comparison to the conventional photonic laser, the plasmonic cavities exhibit ultrasmall modal volume $V_m \sim \lambda^3/10 - \lambda^3/1000$, which enables the control of the strong light-matter interaction and the generation of extremely intense optical fields. Sidiropoulos *et al.*[168] observed the emission pulses shorter than 800 fs from hybrid plasmonic zinc oxide (ZnO) nanowire ($5 < L < 20$ μm, $100 < D < 300$ nm.) lasers (Fig. 17). In such plasmonic lasers, the atomic smoothness of the metallic film is crucial for reducing the modal volume and plasmonic losses.[170] Graphene/ZnO hybrid microcavity has also been shown to be useful to realize plasmon coupled F-P lasing, resulting in the lowered lasing threshold and the remarkably enhanced lasing intensity.[171] Chou *et al.*[172] recently investigated ZnO plasmonic nanolasers on a pseudowedge surface plasmon polariton waveguide formed on a high-quality Ag crystal carved with a subwavelength metallic grating, which allows them to shorten the effective cavity length and to realize single longitudinal-mode lasing.

Compared with optically pumped lasing, reports on the electrically pumped nanolasers are rather few. This is mainly due to the fact that stable and reproducible

production of p-type ZnO nanostructures are still challenging for ZnO micro/nanostructures with a p-n homojunction. Note, however, that Chu *et al.*[173] successfully demonstrated electrically driven FP lasing from n-type ZnO nanowires combined with p-type Sb-doped ZnO nanowires (Fig. 18). An attempt to design and fabricate electrically pumped ZnO nanolasers with p-n heterojunctions[174] as well as those on other II-VI or III-V semiconductors[175–177] has also been reported.

2. Whispering gallery mode *(WGM) lasing*

The FP lasing mentioned in the previous subsection is historically important in view of nanowire photonics. However, a high level of confinement cannot be in principle obtained in FP lasing due to the low reflectivity (R≈15.5 %) at the ZnO/air interfaces. This drawback can be improved by using another kind of resonator mode: WGM. In WGM lasing, the resonance is generated through total internal reflection (TIR) at the cavity boundary. This results in WGM being ideally free from mirror losses as perfect TIR provides a 100 % reflection. Even when perfect TIR occurs in hexagonal microcavities, the light can escape at the corners of the cavity.[178] Figure 19(a) shows a ray with slightly different initial angle of incidence caused by the incident angular fluctuation. The ray is slowly diverging from the central one, eventually reaching the corner on its other side at almost normal incidence. Consequently, it then escapes refractively with probability close to 1, as also shown in the simulated light-field distribution [Fig. 19(b)]. This phenomenon is referred to as the pseudointegrable leakage. In addition, corner diffraction[179] and boundary-wave leakage associated with the presence of evanescent waves[178] are also responsible for partial leakage of light from the hexagonal

cavity. Consequently, the lasing intensity would be distributed with a period angle of π/3, which was confirmed experimentally by Dai *et al*.[180] using a ZnO hexagonal microrod with *D* of 6.67 μm (Fig. 20). The escape rate of the light due to the pseudointegrable leakage in a hexagonal cavity is expected to be nearly inversely proportional to the cavity size *D*.[180] Therefore, the lasing threshold of the hexagonal ZnO cavity were found to show an approximately linear dependence on 1/*D* [Fig. 21(a)].[143,180] A typical lasing threshold for the hexagonal ZnO cavity with $D > 10$ μm is 100-200 kW/cm^2. [143,180,181] It is also interesting to mention the *Q* factor of ZnO WGM microcavities since it is a useful measure of determining the feedback in the resonant cavity. Similar to the case of lasing threshold, the *Q* factor shows a strong dependence on *D* [Fig. 21(b)]. For a sufficiently large (*D* ~12.6 μm) high-quality hexagonal ZnO microdisk, a *Q* factor as high as 3300 has been reported.[181] This value is much larger than that observed commonly in ZnO F-P cavities (*Q*~500),[62] demonstrating that the feedback performance of WGM microcavities is better than that of the F-P ones.

In addition to the hexagonal WGM microcavities, lasing from dodecagonal WGM cavities has also been reported (Fig. 22).[182] During the growth of ZnO microrods by a vapor phase transport method, the deposition area was kept at a very high temperature (~1000 ˚C) so that the evaporated Zn and O atoms have enough energy to bind and diffuse on $(01\bar{1}0)$ and $(\bar{2}110)$ surface evenly, resulting in the dodecagonal microrods with $D <$ ~10 μm [Fig. 22(b)]. Compared to the case of hexagonal cavities with similar sizes, a lower lasing threshold (180 kW/cm^2) and a higher *Q* factor (*Q*~2600) are obtained from the dodecagonal ZnO microrod ($D = 6.35$ μm), as shown in Fig. 23. This is because the WGM optical length in a dodecagonal cavity is longer than that in a hexagonal one with

the same cross-sectional diameter.

There have been a few reports on electrically driven ZnO WGM lasers.[183–185] Recently, Zhou *et al*.[185] reported electrically driven lasing from a system consisting of Ga doped ZnO hexagonal micorowire (ZnO:Ga) with D = 15 μm covered partially with platinum nanoparticles and a p-type GaN substrate (Fig. 24). This ZnO:Ga/GaN heterojunction exhibits electrically driven single-mode lasing with a linewidth of ~0.18 nm, corresponding to the Q factor of ~2169 [Fig. 24(d)]. The WGM lasing characteristics was confirmed from the optical microscopic CCD image as well as the angle-dependent variation of the laser emission intensity (Fig. 25).

VI. GAIN MECHANISM FOR LASING

Two principal gain mechanisms have been believed to be responsible for lasing in ZnO bulk and nanostructures: excitonic and electron-hole plasma (EHP) recombination processes. When the density of electron-hole pairs n_{p} reaches the Mott density n_{M}, the transition from an insulating exciton gas to a metal-like state of an EHP occurs,[186] as shown schematically in Fig. 26.[187] This indicates that E_X^b decreases with n and becomes zero as n reaches n_{M},[188]

$$E_X^b(n_M) = 0. \quad (8)$$

The Mott density can be calculated within various approximations. At zeroth approximation, n_{M} can be regarded as the carrier density at which average exciton-exciton

distance becomes approximately equal to Bohr radius a_{Bohr}, which is given by

$$n_M \approx \frac{1}{a_{\mathrm{Bohr}}^3}. \qquad (9)$$

However, this model tends to overestimate the critical density ($n_M = 1.7 \times 10^{20}$ cm^3 for $a_{\mathrm{Bohr}}^{\mathrm{ZnO}} = 1.8$ nm[22]). Several more refined and experimentally checked models taking into account the electrostatic screening and the many body effect have been proposed.[188–193] However, the estimated value of n_{M} in ZnO at room temperature shows a variation in the range from 3×10^{17} to 6×10^{18} cm^{-3}.[188–192] Its exact determination is of great importance but is still an open question, as will be discussed later (see sec. IV. B).

A. Excitonic lasing

Historically, exciton-related spontaneous and stimulated emission processes in ZnO as well as in other II-IV and III-V direct gap compounds were extensively investigated both experimentally and theoretically in 1970/80s using high-quality bulk single crystals.[194–200] From these investigations, it has been revealed that in ZnO, stimulated emissions with excitonic gain occur when the second particle (exciton, electon, phonon) is involved in the recombination process. Among other processes, the following three emission processes are especially of interest:

(i) exciton-exciton (X-X) recombination

(ii) exciton-electron (X-el) recombination

(iii) exciton-*m*LO phonon (X-*m*LO, m=1,2...) recombination

We will explain the reason why the above excitonic processes show stimulated emission, or population inversion, by considering the optical emission and absorption processes of the X-X scattering.[196]

If the momentum of the photon is neglected, the recombination energy $\hbar\omega$ due to the inelastic interaction between two excitons can be described as[196,197]

$$\hbar\omega = \left(E_g - E_X^b\right) - E_X^b\left(1 - \frac{1}{n^2}\right) - \frac{\hbar^2}{M}\boldsymbol{K}_1 \cdot \boldsymbol{K}_2, \quad n = 2,3,\ldots \quad (10)$$

where $\boldsymbol{K}_1$ and $\boldsymbol{K}_2$ are wave vectors of the initial two excitons, n is the quantum number of the scattered exciton, and M is the exciton mass. When considering the maximum value of $\hbar\omega$, we can replace the last term in Eq. (10) by the mean kinetic energy.[197] Hence, we get

$$\hbar\omega_{\max}^{\mathrm{X-X}} = \left(E_g - E_X^b\right) - E_X^b\left(1 - \frac{1}{n^2}\right) - \frac{3}{2}k_{\mathrm{B}}T, \quad n = 2,3,\ldots \quad (11)$$

where k_{B} is the Boltzmann constant. The resulting emission band is conventionally referred to as the $P(n)$ band.[196,197] As photons and excitons are bosons, the rate of their generation is not only proportional to their numbers but is also increased by unity.[201] The total rate of photon emission w_{e} in the X-X scattering process is given by

$$r_e = AN_{1,K_1}N_{1,K_2}\left(1 + N_{n,K_1+K_2}\right)(1 + N_w), \quad (12)$$

where N_w is the density of photons, $N_{1,K_1}(N_{1,K_2})$ is the density of the initial state of excitons with a wave vector $\boldsymbol{K}_1$ ($\boldsymbol{K}_2$), N_{n,K_1+K_2} is the density of the final n state for the scattered exciton, and $A=A(n,K_1,K_2,\omega)$ is the rate constant containing the optical matrix element and the scattering matrix element. The rate of photo absorption due to an inverse process is given by

$$r_a = A(N_{1,K_1}+1)\big(N_{1,K_2}+1\big)N_{n,K_1+K_2}N_w. \quad (13)$$

If we neglect the losses caused by the escape of photons from the system, the net emission rate is given by subtracting Eq. (13) from Eq. (12),

$$r_{\mathrm{e,net}} = AN_{1,K_1}N_{1,K_2}\big(N_{n,K_1+K_2}+1\big) + A\left(N_{1,K_1}N_{1,K_2} - N_{n,K_1+K_2}\big((N_{1,K_1}+N_{1,K_2}+1\big)\right)N_w. \quad (14)$$

The first and second terms in Eq (14) represent the rates of spontaneous emission $w_{\mathrm{e,spont}}$, and stimulated emission $w_{\mathrm{e,stim}}$, respectively. It is clear that $r_{\mathrm{e,stim}}$ is increased as the population of the final n state for the scattered excitons N_{n,K_1+K_2} is decreased. It is probable that the $n=\infty$ state is empty even in high excitation conditions, meaning that the condition of a population inversion (optical gain) is realized preferentially for $n=\infty$. Hence, in high-quality ZnO crystals with low optical losses, moderate/high optical excitation leads to stimulated emission in the energy region of the $P(\infty)$ line, which is preceded by the transition from a spontaneous $P(2)$ to a $P(\infty)$ process.[195-197,202] From Eq.

(11), one sees that the stimulated $P(\infty)$ line shows a red shift with respect to the recombination energy of the free exciton by the exciton binding energy ($E_X^b = 60$ meV) at low temperatures ($k_BT \sim 0$). The gain mechanism of the X-el and X-mLO processes can be also explained in a similar manner. For example, the population inversion occurs in the X-mLO process provided that there is one exciton and no LO phonon. The temperature dependence of the emission maximum for the X-el and X-mLO (m=1,2) processes is described by[197]

$$\hbar\omega_{\max}^{\mathrm{X-el}} = \left(E_g - E_X^b\right) - \gamma k_B T, \quad (15)$$

$$\hbar\omega_{\max}^{\mathrm{X}-m\mathrm{LO}} = \left(E_g - E_X^b\right) - m\hbar\omega_{\mathrm{LO}} + \left(\frac{5}{2} - m\right)k_B T, \quad (16)$$

where γ is a constant related to the ratio of exciton effective mass over electron effective mass and $\hbar\omega_{\mathrm{LO}}$ quantum energy of the LO phonon ($\hbar\omega_{\mathrm{LO}} = 72$ meV). It has been demonstrated that γ reaches values as high as 7 in the case of the X-el stimulated emission.[197] The X-mLO process is observed preferentially when large volume with low losses are excited, for example, by two-photon absorption because of its relatively low gain.[197]

Although the stimulated emission due to the X-X process was well documented in bulk ZnO single crystals[195–197] and epitaxial layers[202] at temperatures below ~70 K, the claim of its occurrence at room temperature from ZnO thin films[5–8] has been debated.[1,188] This is because the $n \geq 2$ excitonic states become thermally populated with increasing temperature, leading to thermal ionization of excitons as well as an increase of the threshold of the X-X stimulated emission process. It is hence expected that the transition

from the X-X to X-el occurs at temperatures above 100 K.[1] This expectation was indeed confirmed by Uchino and coworkers[203,204] by measuring the temperature-dependent random laser emission with incoherent feedback in micrometer-thick ZnO and Mg_xZn_{1-x} films (Fig. 27), whose lasing spectra represent the ASE or the maximum of the net gain of the medium (see sec. III.A.2).

It should be noted that room-temperature excitonic lasing is not normally observed in nanometer-sized ZnO crystals, such as nanopowders (random laser) and nanowires (F-P cavity), because in these nanocrystals, the optical excitation near the lasing threshold easily reaches the regime of n_M to yield an EHP emission, as will be shown in the next subsection. That is, in order to realize excitonic lasing, the sample size must be comparable to or larger than the diffusion length of the excited carriers (~3μm[186]) to suppress the formation of the high-density photoexcited carrier region that exceeds n_M.[203] The effect of size on the gain mechanism is also recognized in WGM lasing. Hexagonal or dodecagonal ZnO microrods with a diameter $D \geq$ ~8 μm shows a feature of excitonic WGM lasing, whose peak positions depend hardly on the excitation density.[180–182] On the other hand, the lasing spectra from those with $D \leq$ ~3 μm exhibit a substantial red-shift and broadening with increasing excitation intensity, which is a typical characteristic of an EHP emission[182] (for details, see the next subsection).

B. Electron-hole plasma (EHP) lasing

First, we revisit what happens when the density of free excitons n_x increases during photoexcitation. For an isolated free exciton, the attractive Coulomb potential is given by

$$U(\mathrm{r}) = -\frac{e^2}{4\pi\varepsilon_r\varepsilon_0 r}, \qquad (17)$$

where r is the distance between electron and hole, and ε_0 and ε_r are the dielectric constants of vacuum and the relative dielectric constant, respectively. As the temperature of the system increases, some of the excitons are assumed to be ionized, resulting in a certain number of free electron-hole pairs n_p. Accordingly, the interaction potential should be replaced by the following Yukawa potential to include the effect of effective screening of the Coulomb interaction,[201]

$$U_s(\mathrm{r}) = -\frac{e^2}{4\pi\varepsilon_r\varepsilon_0 r}\exp(-\frac{r}{\lambda_s}), \qquad (18)$$

where λ_s the screening length. That is, λ_s is infinite for an isolated free exciton, whereas λ_s becomes shorter with increasing n_p. When λ_s reaches a_{Bohr} ($a_{\mathrm{Bohr}}^{\mathrm{ZnO}} = 1.8$ nm[22]), the attractive interaction between a single electron and a hole is screened, i.e., $E_X^b = 0$, eventually leading to the transition of the exciton gas to an EHP. If we have knowledge of λ_s as a function of n_p and T, we can estimate n_M at any temperature. However, it is rather a difficult task to get exact knowledge of $\lambda_s(n_p, T)$, causing a wide range of reported values of n_M, as noted earlier. Versteegh *et al.*[189] numerically calculated $\lambda_s(n_p, T)$ using the following formula,

$$\lambda_{s,i} = \sqrt{\frac{\varepsilon_r\varepsilon_0}{e^2}\frac{\partial F_i}{\partial n_p}}, \qquad (19)$$

$$\lambda_s^{-2} = \sum_i \lambda_{s,i}^{-2}, \quad (20)$$

$$n_p = n_i = \frac{1}{2\pi^2}\left(\frac{2m_i}{\hbar^2}\right)^{3/2} \int_0^\infty d\varepsilon\sqrt{\varepsilon}\,\frac{1}{\exp\left[\left(\varepsilon - F_i\right)/k_{\mathrm{B}}T\right] + 1}, \quad (21)$$

where i stands for e (electron) or h (hole), F_i is the quasi-Fermi levels (chemical potentials) measured from the corresponding band extremes. Thus, in this case, one has to define two separate quasi-Fermi levels for electrons in the conduction band ($\mu_{\mathrm{e}}^{'}$, F_{e}) and for holes ($\mu_{\mathrm{h}}^{'}$, F_{h}) in the valence band (see Fig. 28). The resulting relationship between λ_{s} and n_{p} at 300 K are given in Fig. 29, demonstrated that $n_{\mathrm{M}} = 1.5\times10^{18}$ cm^{-3}. This procedure reported by Versteegh *et al.*[189] probably yields the most reliable and reasonable value for n_{M}, in consistent with the experimentally estimated upper limit of n_{M} ($n_{\mathrm{M}} < 2–3\times10^{18}$ cm^{-3}).[191]

The increase in n_{p} also leads to a reduction of the bandgap energy or a band gap renormalization (BGR), which does not affect λ_{s} at a certain carrier density.[189] The resulting reduced band gap is often described as $E_{\mathrm{g}}^{'}$ (see Fig. 28) to distinguish it from the bandgap without renormalization E_{g}.[186] The BGR results from many-body effects including exchange and correlation effects.[186] In uni-polar plasma of electrons in highly chemically doped ZnO,[205–207] the expected band-gap narrowing is not actually observed in the optical gap of ZnO as it is largely compensated by band filling of the conduction band (Burstein-Moss effect).[208,209] Furthermore, even in an EHP there still exists the Coulomb interaction between the photogenerated conduction-band electron and valence-band hole.[186] This leads to an enhancement of the optical absorption and luminescence near the Fermi edge coined as Femi edge singularity and Mahan exciton,[210] which is still

a topic of intense research in the field of highly doped and highly excited semiconductors.[192,211–215]

Next, we turn to the condition of the optical gain in an EHP. The Femi-Dirac distribution function $f(E)$ for electrons with energy E_1 in the valence band and for those with energy E_2 in the conduction band can be written by

$$f_{\mathrm{v}}(E_1) = \frac{1}{\exp\left(\frac{E_1 - \mu_{\mathrm{h}}^{'}}{k_{\mathrm{B}}T}\right) + 1}, \quad (22)$$

$$f_{\mathrm{c}}(E_2) = \frac{1}{\exp\left(\frac{E_2 - \mu_{\mathrm{e}}^{'}}{k_{\mathrm{B}}T}\right) + 1}, \quad (23)$$

As for the interband processes, the rates of stimulated emission r_{stim} and absorption r_{abs} for light with a spectral distribution $u(\nu)$ are given by[201]

$$r_{\mathrm{stim}}(h\nu) = B_{21}u(\nu)\rho(\nu)f_e(\nu), \quad (24)$$

$$r_{\mathrm{abs}}(h\nu) = B_{12}u(\nu)\rho(\nu)f_a(\nu), \quad (25)$$

where B_{21} and B_{12} are the Einstein coefficients of stimulated emission and absorption, respectively, $\rho(\nu)$ is the joint density of electron and hole states in the bands, and $f_e(\nu) = f_{\mathrm{c}}(E_2)[1 - f_{\mathrm{v}}(E_1)]$ and $f_a(\nu) = f_{\mathrm{v}}(E_1)[1 - f_{\mathrm{c}}(E_2)]$ are the probabilities of photon emission and absorption, respectively. Considering the equality $B_{12} = B_{21} = B$, we obtain the resulting rate of observable stimulated emission:

$$R_{\mathrm{stim}}(h\nu) = r_{\mathrm{stim}}(h\nu) - r_{\mathrm{abs}}(h\nu) = Bu(\nu)\rho(\nu)[f_{\mathrm{c}}(E_2) - f_{\mathrm{v}}(E_1)]. \quad (26)$$

Hence, the sign of $R_{\mathrm{stim}}(h\nu)$ is determined by the sign of the term $f_{\mathrm{c}}(E_2) - f_{\mathrm{v}}(E_1)$. From Fig. 28, one sees that

$$E_2 = E_1 + h\nu, \quad (27)$$

$$\mu_{\mathrm{e}}^{'} = \mu_{\mathrm{h}}^{'} + E_{\mathrm{g}}^{'} + F_{\mathrm{h}} + F_{\mathrm{e}}. \quad (28)$$

By using Eqs. (22), (23), (27) and (28), one finds that sign of the term $f_{\mathrm{c}}(E_2) - f_{\mathrm{v}}(E_1)$ is eventually controlled by the following numerator term:[201]

$$1 - \exp\left(\frac{h\nu - E_{\mathrm{g}}^{'} - F_{\mathrm{h}} - F_{\mathrm{e}}}{k_{\mathrm{B}}T}\right). \quad (29)$$

It thus follows that $R_{\mathrm{stim}}(h\nu)$ becomes positive when $h\nu < E_{\mathrm{g}}^{'} + F_{\mathrm{h}} + F_{\mathrm{e}}$, which limits the high-energy end of the gain. One also notices from Fig. 28 that the lowest photon energy amplified in the quasi-equilibrium state is $h\nu = E_{\mathrm{g}}^{'}$. Consequently, the optical gain in an EHP is expected to occur in the following energy range:

$$E_{\mathrm{g}}^{'} < \ h\nu < E_{\mathrm{g}}^{'} + F_{\mathrm{h}} + F_{\mathrm{e}} = \mu_{\mathrm{e}}^{'} - \mu_{\mathrm{h}}^{'}. \quad (30)$$

The term $\mu_{\mathrm{e}}^{'} - \mu_{\mathrm{h}}^{'}$ is referred to as the chemical potential of an EHP system.[186] In the EHP regime, the observed emission spectra show a substantial red-shift and spectral

broadening with increasing excitation intensity due to the reduction of E_g'.[186,201]

Then the EHP lasing occurs in ZnO when an appropriate feedback mechanism is provided. Theoretical calculations based on quantum many-body theory have demonstrated that the F-P laser modes in ZnO nanowires[190] and the random laser modes in ZnO nanopowders[216] result mostly from the EHP lasing because of their relatively high threshold carrier density $n_p^{th} \geq \sim 10^{20}$ cm^{-3} > n_M. In ZnO nanostructures, however, the gain mechanism depends strongly on their shape, size and optical quality, as already mentioned in sec. IV.A. Indeed, highly faceted ZnO rods with a lower threshold show a transition in the gain mechanism from excitonic to EHP recombination with increasing excitation intensity,[65,217] which can be identified by the excitation intensity-dependent change in the PL spectra and their decay dynamics. Figure 30 show examples of highly faceted ZnO rods and their time-resolved PL spectra at 300 K.[65] A broad spontaneous emission with time constant with several hundreds of picoseconds is seen at ~380 nm (3.26 eV) under low pump intensity. The threshold for excitonic lasing was observed to occur at ~45 μJ/cm^2, showing narrow F-P lasing modes with line width ~0.4 nm and rise and decay times in the range 4-5 ps. The delay in the onset of the excitonic lasing could be due to the relatively long (> 5 ps) time necessary for the relatively weak excitonic interaction to produce sufficient scattering events required for optical gain.[217] Optical pump-THz measurements also supported such slow evolution of free carriers to excitons in the 10 to 100 ps following photo-excitation.[191] As the pump intensity increases to ~90 μJ/cm^2, the spectrum becomes broad and red-shifted, accompanied by substantial shortening of rise (~1ps) and decay (2–3 ps) times. This can be interpreted in term of a very fast (<100 fs) cooling of the hot carriers to a quasi-thermal equilibrium.[191,217] We

should also note that the reverse transition, i.e., from EHP to excitonic lasing, is observed during the decay process of the EHP emission from ZnO nanostructures with low excitonic threshold (~40 μJ/cm^2).[218] Fig. 31. shows the time-resolved PL from these ZnO nanostructures in the EHP regime created under high (~126 μJ/cm^2) excitation fluence. The PL peak first shift to the red at 1 ps, and then start shrinking back to the from 2 ps, resulting in a structured emission observed in the excitonic lasing regime at 10 ps. This temporal change in the PL spectra results from the faster decay (2–3 ps) of the EHP emission and the subsequent decrease in the free carrier concentration and a consequential band gap recovery, leading to the excitonic lasing.[218] These results indicate that excitons can be formed as a result of the thermalization and cooling of the hot EHP gas..

V. CONCLUSIONS

In this Tutorial, we have attempted to create a picture of creation, recombination and screening of excitons in ZnO thin films and micro/nanostructures in view of excitonic and EHP lasing. It has been shown that photoexcitation and recombination in ZnO are very versatile and rich in the resulting stimulated emission processes. This versatility stems partly from their diverse morphologies from one- dimensional to three-dimensional structures in the nanometer to micrometer range, which enables various kinds of feedback, including random lasing in an aggregation of nanoparticles, F-P lasing in a nanowire, and WGM lasing in a hexagonal plate. The other factor of versatility derives from its relatively large exciton binding energy of 60 meV, which is larger than k_BT at room temperature (~26 meV) and hence tempts us to ascribe stimulated emission at room temperature to excitonic processes. It should be noted, however, that for n_p larger than n_M, the excitonic gain does not occur, but EHP related gain begins to settle in. Thus, the exact estimation

of n_p is crucial to determine which gain process operates in the ZnO micro and nanostructures of interest. Roughly speaking, room-temperature lasing observed in ZnO nanowires and nanoparticles is mostly ascribed to EHP lasing due to their relatively high threshold carrier density. Of course, it would be possible to observe excitonic lasing from ZnO nanostructures if one can reduce the threshold carrier density below n_M, for example, by controlling their size and shape, as in the case of WGM excitonic lasing, or by using surface plasmon modes. Thus, ZnO is still an interesting and challenging wide band gap semiconductor in terms of lasing and related photoelectronic phenomena.

AUTHOR DECLARATIONS

Conflict of Interest

The authors have no conflicts to disclose.

Author Contributions

Aika Tashiro: Data curation (equal); Investigation (equal); Writing– review & editing (equal). **Yutaka Adachi**: Data curation (equal); Investigation (equal). **Takashi Uchino**: Data curation (equal); Conceptualization (lead); Writing– original draft (lead); Writing– review & editing (lead).

DATA AVAILABILITY

The data shown in Fig. 1 are available from the corresponding author upon reasonable request.

References

[1] G. Heiland, E. Mollwo, F. Stöckmann, in *Solid State Physics*, edited by F. Seitz and D. Turnbull (Academic, New York, 1959), Vol. 8. pp.191-323.

[2] C. Klingshirn, J. Fallert, H. Zhou, J. Sartor, C. Thiele, F. Maier-Flaig, D. Schneider, and H. Kalt, 65 years of ZnO research – old and very recent results, Phys. Stat. Solidi B **247**, 1424 (2010).

[3] D. C. Reynolds, D. C. Look, B. Jogai, C. W. Litton, G. Cantwell, and W. C. Harsch, Valence-band ordering in ZnO, Phys. Rev. B **60**, 2340 (1999).

[4] A. Teke, Ü. Özgür, S. Doğan, X. Gu, H. Morkoç, B. Nemeth, J. Nause, and H. O. Everitt, Excitonic fine structure and recombination dynamics in single-crystalline ZnO, Phys. Rev. B **70**, 195207 (2004)

[5] D. M. Bagnall, Y. F. Chen, Z. Zhu, and T. Yao, S. Koyama, M. Y. Shen, and T. Goto, Optically pumped lasing of ZnO at room temperature, Appl. Phys. Lett. **70**, 2230 (1997).

[6] D. M. Bagnall, Y. F. Chen, Z. Zhu, T. Yao, M. Y. Shen and T. Goto, High temperature excitonic stimulated emission from ZnO epitaxial layers, Appl. Phys. Lett. **73**, 1038 (1998).

[7] P. Zu, Z. K. Tang, G. K. L. Wong, M. Kawasaki, A. Ohtomo, H. Koinuma, Y. Segawa, Ultraviolet spontaneous and stimulated emissions from ZnO microcrystallite thin films at room temperature, Solid State Commun. **103**, 459 (1997).

[8] Z. K. Tang, G. K. L. Wong, P. Yu, M. Kawasaki, A. Ohtomo, H. Koinuma, and Y. Segawa, Room-temperature ultraviolet laser emission from self-assembled ZnO microcrystallite thin films, Appl. Phys. Lett. **72**, 3270 (1998).

[9] H. Cao, Y. G. Zhao, S. T. Ho, E. W. Seelig, Q. H. Wang, and R. P. H. Chang, Random laser action in semiconductor powder, Phys. Rev. Lett. **82**, 2278 (1999).

[10] M. H. Huang, S. Mao, H. Feick, H. Yan, Y. Wu, H. Kind, E. Weber, R. Russo, and P. Yang, Room-temperature ultraviolet nanowire nanolasers, Science **292**, 1897 (2001).

[11] T. Makino, C. H. Chia, Nguen T. Tuan, H. D. Sun, and Y. Segawa, M. Kawasaki, A. Ohtomo, and K. Tamura, H. Koinuma, Room-temperature luminescence of excitons in ZnO/(Mg,Zn)O multiple quantum wells on lattice-matched substrates, Appl. Phys. Lett. **77**, 975 (2000).

[12] R. Yan, D. Gargas, and P. Yang, Nanowire photonics, Nat. Photon. **3**, 569 (2009).

[13] D. Vanmaekelbergh and L. K. van Vugt, ZnO nanowire lasers, Nanoscale **3**, 2783 (2011).

[14] M. Willander, O. Nur, Q. X. Zhao, L. L. Yang, M. Lorenz, B. Q. Cao, J. Z. Pérez, C. Czekalla, G. Zimmermann, M. Grundmann, Zinc oxide nanorod based photonic devices: recent progress in growth, light emitting diodes and lasers, Nanotechnol. **20**, 33 (2009).

[15] D. S. Wiersma, The physics and applications of random lasers, Nat. Phys. **4**, 359 (2008).

[16] D. S. Wiersma, Disordered photonics, Nat. Photon. **7**, 188 (2013).

[17] N. Padiyakkuth, S. Thomas, R. Antoine, and N. Kalarikkal, Recent progress and prospects of random lasers using advanced materials, Mater. Adv. **3**, 6687 (2022).

[18] F. Li, L. Orosz, O. Kamoun, S. Bouchoule, C. Brimont, P. Disseix, T. Guillet, X. Lafosse, M. Leroux, J. Leymarie, M. Mexis, M. Mihailovic, G. Patriarche, F. Réveret, D. Solnyshkov, J. Zuniga-Perez, and G. Malpuech, From excitonic to

photonic polariton condensate in a ZnO-based microcavity, Phys. Rev. Lett. **110**, 196406 (2013).

[19] D. Sanvitto and S. Kéna-Cohen, The road towards polaritonic devices, Nat. Mater. **15**, 1061(2016).

[20] Y. Zhang, X. Zhang, B. Tang, C. Tian, C. Xu, H. Dong and W. Zhou, Realization of an all-optically controlled dynamic superlattice for exciton–polaritons, Nanoscale **10**, 14082 (2018).

[21] C. Kan, Y. Wu, J. Xu, P. Wan, and M. Jiang, Opt. Exp. **29**, 5795 (2021).

[22] Ü. Özgür, Ya. I. Alivov, C. Liu, A. Teke, M. A. Reshchikov, S. Doğan, V. Avrutin, S.-J. Cho, and H. Morkoç, A comprehensive review of ZnO materials and devices, J. Appl. Phys, **98**, 041301 (2005).

[23] A. B. Djurišić and Y. H. Leung, Optical Properties of ZnO Nanostructures, Small **2**, 944 (2006).

[24] L. Schmidt-Mende, J. L. MacManus-Driscoll, ZnO – nanostructures, defects, and devices, Mater. Today **10**, 40 (2007).

[25] C. Klingshirn, ZnO: From basics towards application, Phys. Stat. Solidi B **244**, 3027 (2007).

[26] A. B. Djurišić, A. M. C. Ng, and X. Y .Chen, ZnO nanostructures for optoelectronics: Material properties and device applications, Prog. Quant. Electron. **34**, 191 (2010).

[27] Z. L. Wang, ZnO nanowire and nanobelt platform for nanotechnology, Mater. Sci. Eng. R **64**, 33 (2009).

[28] J. A. Spencer, A. L. Mock, A. G. Jacobs, M. Schubert, Y. Zhang, and M. J. Tadjer, A review of band structure and material properties of transparent conducting and

semiconducting oxides: Ga_2O_3, Al_2O_3, In_2O_3, ZnO, SnO_2, CdO, NiO, CuO, and Sc_2O_3, Appl. Phys. Rev. **9**, 011315 (2022).

[29] S. Rahaa and Md. Ahmaruzzaman, ZnO nanostructured materials and their potential applications: progress, challenges and perspectives, Nanoscale Adv. 4, 1868 (2022).

[30] W. Y. Liang and A. D. Yoffe, Transmission spectra of ZnO single crystals, Phys. Rev. Lett. **20**, 59 (1968).

[31] S. F. Chichibu, A. Tsukazaki, M. Kawasaki, K. Tamura, Y. Segawa, T. Sota, H. Koinuma, Photoreflectance spectra of a ZnO heteroepitaxial film on the nearly lattice matched $ScAlMgO_4$ (0001) substrate grown by laser molecular-beam epitaxy, Appl. Phys. Lett. **80**, 2860 (2002).

[32] D. Y. Lin, H. J. Lin, J. S. Wu, W. C. Chou, C. S. Yang, and J. S. Wang , A comprehensive study of temperature-dependent reflectance and photoluminescence of $Zn_{1-x}Mn_xO$ thin films grown on c-Al_2O_3, J. Appl. Phys. **105,** 053506 (2009).

[33] D. W. Hamby, D. A. Lucca, and M. J. Klopfstein, Temperature dependent exciton photoluminescence of bulk ZnO, J. Appl. Phys. **93**, 3214 (2003).

[34] J. Rodrigues, N. B. Sedrine, M. R. Correia, and T. Monteiro, Photoluminescence investigations of ZnO micro/nanostructures, Mater. Today Chem. **16**, 100243 (2020).

[35] T. Nobis, E.M. Kaidashev, A. Rahm, M. Lorenz, J. Lenzner, and M. Grundmann, Spatially inhomogeneous impurity distribution in ZnO micropillars, Nano Lett. **4**, 797 (2004).

[36] L. J. Brillson, W. T. Ruane, H. Gao, Y. Zhang, J. Luo, H. von Wenckstern, and M.

Grundmann, Spatially-resolved cathodoluminescence spectroscopy of ZnO defects, Mater. Sci. Semicond. Process. **57**, 197 (2017).

[37] J. I. Pankove, Optical Processes in Semiconductors (Dover, New York, 1971), p. 36.

[38] V. Craciun, J. Elders, J. G. E. Gardeniers, and Ian W. Boyd, Characteristics of high quality ZnO thin films deposited by pulsed laser deposition, Appl. Phys. Lett. **65**, 2963 (1994).

[39] J.-J. Wu and Sai-Chang Liu, Catalyst-free growth and characterization of ZnO Nanorods, J. Phys. Chem. B **106**, 9546 (2002).

[40] B. D. Viezbicke, S. Patel, B. E. Davis, and D. P. Birnie III, Evaluation of the Tauc method for optical absorption edge determination: ZnO thin films as a model system, Phys. Status Solidi B **252**, 1700 (2015).

[41] R. C. Rai, M. Guminiak, S. Wilser, B. Cai, and M. L. Nakarmi, Elevated temperature dependence of energy band gap of ZnO thin films grown by e-beam deposition, J. Appl, Phys. **111**, 073511 (2012).

[42] Y. S. Park, C. W. Litton, T. C. Collins, and D. C. Reynolds, Exciton spectrum of ZnO, Phys. Rev. **143**, 512 (1966).

[43] J. F. Muth and R. M. Kolbas, A. K. Sharma, S. Oktyabrsky, and J. Narayan, Excitonic structure and absorption coefficient measurements of ZnO single crystal epitaxial films deposited by pulsed laser deposition, J. Appl. Phys. **85**, 7884 (1999).

[44] D. G. Thomas, The exciton spectrum of zinc oxide, J. Phys. Chem. Solids **15**, 86 (1960).

[45] Y. P. Varshni, Temperature Dependence of the Energy Gap in Semiconductors. Physica, **34**, 149 (1967).

[46] P. Lautenschlager, M. Garriga, S. Logothetidis, and M. Cardona, Interband critical points of GaAs and their temperature dependence, Phys. Rev. B **35**, 9174 (1987).

[47] G. D. Cody, in Hydrogenated Amorphous Silicon, edited by J. I. Pankove, Semiconductors and Semimetals, Vol. 21, Part b (Academic, New York, 1984), Chap. 2, pp. 42–47.

[48] L. Wang and N. C. Giles, Temperature dependence of the free-exciton transition energy in zinc oxide by photoluminescence excitation spectroscopy, J. Appl. Phys. **94**, 973 (2003).

[49] A. Tereshchenko, M. Bechelany, R. Viter, V. Khranovskyy, V. Smyntyna, N. Starodub, R. Yakimova, Optical biosensors based on ZnO nanostructures: advantages and perspectives. A review, Sens. Actuators B Chem. **229**, 664 (2016).

[50] J. Rodrigues, S. O. Pereirq, J. Zanoni, C. R. M. Brás, F. M. Costa, and T. Monteiro, ZnO transducers for photoluminescence-based biosensors: A Review, Chemosensors **10**, 39 (2022).

[51] B. K. Meyer, H. Alves, D. M. Hofmann, W. Kriegseis, D. Forster, F. Bertram, J. Christen, A. Hoffmann, M. Straßburg, M. Dworzak, U. Haboeck, and A. V. Rodina, Bound exciton and donor–acceptor pair recombinations in ZnO, Phys. Status 52

[52] M. R. Wagner, G. Callsen, J. S. Reparaz, J.-H. Schulze, R. Kirste, M. Cobet, I. A. Ostapenko, S. Rodt, C. Nenstiel, M. Kaiser, A. Hoffmann, A. V. Rodina, M. R. Phillips, S. Lautenschläger, S. Eisermann, and B. K. Meyer, Bound excitons in ZnO: Structural defect complexes versus shallow impurity centers, Phys. Rev. B **84**, 035313 (2011).

[53] R. Heinhold, A. Neiman, J. V. Kennedy, A. Markwitz, R. J. Reeves, and M. W. Allen, Hydrogen-related excitons and their excited-state transitions in ZnO, Phys.

Rev. B **95**, 054120 (2017).

[54] J. Grabowska, A. Meaney, K. K. Nanda, J.-P. Mosnier, M. O. Henry, J.-R. Duclère, and E. McGlynn, Surface excitonic emission and quenching effects in ZnO nanowire/nanowall systems: Limiting effects on device potential, Phys. Rev. B **71**, 115439 (2005).

[55] L. Wischmeier, T. Voss, I. Rückmann, J. Gutowski, A. C. Mofor, A. Bakin, and A. Waag, Dynamics of surface-excitonic emission in ZnO nanowires, Phys. Rev. B **74**, 195333 (2006).

[56] M. Biswas, Y. S. Jung, H. K. Kim, K. Kumar, G. J. Hughes, S. Newcomb, M. O. Henry, and E. McGlynn, Microscopic origins of the surface exciton photoluminescence peak in ZnO nanostructures, Phys. Rev. B **83**, 235320 (2011).

[57] M. Schirra, R. Schneider, A. Reiser, G. M. Prinz, M. Feneberg, J. Biskupek, U. Kaiser, C. E. Krill, K. Thonke, and R. Sauer, Stacking fault related 3.31-eV luminescence at 130-meVacceptors in zinc oxide, Phys. Rev. B **77**, 125215 (2008).

[58] D. Tainoff, B. Masenelli, P. Mélinon, A. Belsky, G. Ledoux, D. Amans, C. Dujardin, N. Fedorov, and P. Martin, Competition between exciton-phonon interaction and defects states in the 3.31 eV band in ZnO, Phys. Rev. B **81**, 115304 (2010).

[59] H. He, Q. Yang, C. Liu, L. Sun, and Z. Ye, Size-dependent surface effects on the photoluminescence in ZnO nanorods, J. Phys. Chem. C **115**, 1, 58 (2011).

[60] L. Sun, H. He, S. Li, and Z. Ye, Annealing-induced changes of the 3.31 eV emission in ZnO nanorods, Appl. Phys. A **115**, 879 (2014).

[61] J. Rodrigues, T. Holz, R. F. Allah, D. Gonzalez, T. Ben, M. R. Correia, T. Monteiro, and F. M. Costa, Effect of N_2 and H_2 plasma treatments on band edge emission of ZnO microrods, Sci. Rep. **5**, 10783 (2015).

[62] D. J. Sirbuly, M. Law, H. Yan, and P. Yang, Semiconductor nanowires for subwavelength photonics integration, J. Phys. Chem. B **109**, 32, 15213 (2005).

[63] S. L. Chen, S. K. Lee, W. M. Chen, H. X. Dong, L. Sun, Z. H. Chen, and I. A. Buyanova, On the origin of suppression of free exciton no-phonon emission in ZnO tetrapods, Appl. Phys. Lett. **96**, 033108 (2010).

[64] J. Fallert, R. Hauschild, F. Stelzl, A. Urban, M. Wissinger, H. Zhou, C. Klingshirn, and H. Kalt, Surface-state related luminescence in ZnO nanocrystals., J. Appl. Phys. **101**, 073506 (2007).

[65] W. M. Kwok, A. B. Djurišić, Y. H. Leung, W. K. Chan, D. L. Phillips, H. Y. Chen, C. L. Wu, S. Gwo, and M. H. Xie, Study of excitonic emission in highly faceted ZnO rods, Chem. Phys. Lett. **412**, 141 (2005).

[66] K. Appavoo, X. Liu, V. Menon, and M. Y. Sfeir, Excitonic lasing in solution-processed subwavelength nanosphere assemblies, Nano Lett. **16**, 2004 (2016).

[67] P. B. Djurišić, W. C. H. Choy, V. A. L. Roy, Y. H. Leung, C. Y. Kwong, K. W. Cheah, T. K. Gundu Rao, W. K. Chan, H. Fei Lui, C. Surya, Photoluminescence and electron paramagnetic resonance of ZnO tetrapod structure, Adv. Funct. Mater. **14**, 856 (2004).

[68] G. Z. Xing, D. D. Wang, B. Yao, A. Q. Lloyd, F. Nien, and Y. S. Yan, Structural characteristics, low threshold ultraviolet lasing and ultrafast carrier dynamics in high crystalline ZnO nanowire arrays, Chem. Phys. Lett. **515**, 132 (2011).

[69] S.-K. Lee, S. L. Chen, D. Hongxing, L. Sun, Z. Chen, W. M. Chen, and I. A. Buyanova, Long lifetime of free excitons in ZnO tetrapod structures, Appl. Phys. Lett. **96**, 083104 (2010).

[70] J. Lapp, D. Thapa, J. Huso, A. Canul, M. G. Norton, M. D. McCluskey, and L.

Bergman, Enhancement of the ultraviolet photoluminescence of ZnO films: Coatings, annealing, and environmental exposure studies, AIP Advances **10**, 085217 (2020).

[71] W. Shan, W. Walukiewicz, J. W. Ager III, K. M. Yu, H. B. Yuan, H. P. Xin, G. Cantwell, and J. J. Song, Nature of room-temperature photoluminescence in ZnO, Appl. Phys. Lett. **86**, 191911 (2005).

[72] Y. Yang, X. W. Sun, B. K. Tay, Peter H. T. Cao1, J. X. Wang, and X. H. Zhang, Revealing the surface origin of green band emission from ZnO nanostructures by plasma immersion ion implantation induced quenching, J. Appl. Phys. **103**, 064307 (2008).

[73] M. Li, G. Xing, G. Xing, B. Wu, T. Wu, X. Zhang, and T. C. Sum, Origin of green emission and charge trapping dynamics in ZnO nanowires, Phys. Rev. B **87**, 115309 (2013).

[74] X. Zhou, Q. Kuang, Z.-Y. Jiang, Z.-X. Xie, T. Xu, R.-B. Huang, and L.-S. Zheng, The origin of green emission of ZnO microcrystallites: surface-dependent light emission studied by cathodoluminescence, J. Phys. Chem. C **111**, 12091 (2007).

[75] A. Gokarna1, R. Aad, J. Zhou, K. Nomenyo, A. Lusson, P. Miska, and G. Lerondel, On the origin of the enhancement of defect related visible emission in annealed ZnO micropods, J. Appl. Phys. **126**, 145104 (2019).

[76] J. A. Röhr, J. Sá, and S, J. Konezny The role of adsorbates in the green emission and conductivity of zinc oxide, Commun. Chem. **2**, 52 (2019).

[77] M. Zhang, F. Averseng, F. Haque, P. Borghetti, J.-M. Krafft, B. Baptiste, G. Costentin and S. Stankic, Defect-related multicolour emissions in ZnO smoke: from violet, over green to yellow, Nanoscale **11**, 5102 (2019).

[78] J. Zhou, K. Nomenyo, C. C. Cesar, A. Lusson, A. Schwartzberg, C.-C. Yen, W.-Y. Woon, and G. Lerondel, Giant defect emission enhancement from ZnO nanowires through desulfurization process, Sci. Rep. **10**, 4237 (2020).

[79] R. Müller, M. Mangold, F. Huber, M. Schreck, U. Herr, and K. Thonke, Fe–Li complex emission in ZnO, J. Appl. Phys. **129**, 085701 (2021).

[80] J. V. Foreman, H. O. Everitt, J. Yang and J. Liu, Influence of temperature and photoexcitation density on the quantum efficiency of defect emission in ZnO powders, Appl. Phys. Lett. **91**, 011902 (2007).

[81] Li Ge, Y. D. Chong, and A. Douglas Stone, Steady-state ab initio laser theory: Generalizations and analytic results, Phys. Rev. A **82**, 063824 (2010).

[82] H. Cao, R. Chriki, S. Bittner, A. A. Friesem, and N. Davidson, Complex lasers with controllable coherence, Nat. Rev. Phys. **1**, 156 (2019).

[83] A. Forbes, M. de Oliveira, and M. R. Dennis, Structured light, Nat. Photon. **15**, 253 (2021).

[84] D. Saxena, A. Arnaudon, O. Cipolato, M. Gaio, A. Quentel, S. Yaliraki, D. Pisignano, A. Camposeo, M. Barahona, and R. Sapienza, Sensitivity and spectral control of network lasers, Nat. Commun. **13**, 6493 (2022)

[85] M. C. T. Bahaa and E. A Saleh, Fundementals of Photonics (Jonh Wiley and Sons Inc., 1991).

[86] M. A. Noginov, G. Zhu, A. M. Belgrave, R. Bakker, V. M. Shalaev, E. E. Narimanov, S. Stout, E. Herz, T. Suteewong, and U. Wiesner, Demonstration of a spaser-based nanolaser, Nature **460**, 1110 (2009).

[87] B. Bahari, A. Ndao, F. Vallini, A. El Amili, Y. Fainman, B. Kanté, Nonreciprocal lasing in topological cavities of arbitrary geometries, Science **358**, 636 (2017).

[88] M. A. Bandres, S. Wittek, G. Harari, M. Parto, J. Ren, M. Segev, D. N. Christodoulides, and M. Khajavikhan, Topological insulator laser: Experiments, Science **359**, eaar4005 (2018).

[89] S. Gottardo, R. Sapienza, P. D. García, A. Blanco, D. S. Wiersma, and C. López, Resonance-driven random lasing, Nat. Photon. **2**, 429 (2008).

[90] H. Cao, Lasing in random media, Waves Random Media **13**, R1 (2003).

[91] M. A. Noginov, Solid-State Random Lasers (Springer, 2005).

[92] A. Boschetti, A. Taschin, P. Bartolini, A. K. Tiwari, L. Pattelli, R. Torre, and D. S. Wiersma, Spectral super-resolution spectroscopy using a random laser, Nat. Photon. **14**, 177 (2020).

[93] R. Sapienza, Determining random lasing action, Nat. Rev. Phys. **1**, 690 (2019).

[94] R. Sapienza, Controlling random lasing action, Nat. Phys. **18**, 976 (2022).

[95] F. Luan, B. Gu, A. S. L. Gomes, K. T. Yong, S. Wen, and P. N. Prasad, Lasing in nanocomposite random media, Nano Today **10**, 168 (2015).

[96] L. Sznitko, J. Mysliwiec, and A. Miniewicz The role of polymers in random lasing, J. Polym. Sci. B **53**, 951 (2015).

[97] A. S. L. Gomes, A. L. Moura, C. B. de Araújo, and E. P. Raposo, Recent advances and applications of random lasers and random fiber lasers, Prog. Quantum Electron. **78**, 100343 (2021).

[98] N. Padiyakkuth, S. Thomas, R. Antoine, and N. Kalarikkal, Recent progress and prospects of random lasers using advanced materials, Mater. Adv. **3**, 6687 (2022).

[99] H. Cao, Y. G. Zhao, H. C. Ong, S. T. Ho, J. Y. Dai, J. Y. Wu, and R. P. H. Chang, Ultraviolet lasing in resonators formed by scattering in semiconductor polycrystalline films, Appl. Phys. Lett. **73**, 3656 (1998).

[100] H. Cao, J. Y. Xu, D. Z. Zhang, S.-H. Chang, S. T. Ho, E. W. Seelig, X. Liu, and R. P. H. Chang, Spatial Confinement of Laser Light in Active Random Media, Phys. Rev. Lett. **84**, 5584 (2000).

[101] H. Cao and Y. Eliezer, Harnessing disorder for photonic device applications, Appl. Phys. Rev. **9**, 011309 (2022).

[102] V. Milner and A. Z. Genack, Photon localization laser: low-threshold lasing in a random amplifying layered medium via wave localization, Phys. Rev. Lett. **94**, 073901(2005).

[103] P. Stano and P. Jacquod, Suppression of interactions in multimode random lasers in the Anderson localized regime, Nat. Photon. **7**, 66 (2013).

[104] H. E. Türeci, L. Ge, S. Rotter, and A. D. Stone, Strong interactions in multimode random lasers, Science **320**, 643 (2008).

[105] M. Leonetti, C. Conti, and C. Lopez, The mode-locking transition of random lasers, Nat. Photon. **5**, 615 (2011).

[106] F. Antenucci, G. Lerario, B. S. Fernandéz, L. De Marco, M. De Giorgi, D. Ballarini, D. Sanvitto, and L, Leuzzi, Demonstration of self-starting nonlinear mode locking in random lasers, Phys. Rev. Lett. **126**, 173901(2021).

[107] S. Schönhuber, M. Brandstetter, T. Hisch, C. Deutsch, M. Krall, H. Detz, A. M. Andrews, G. Strasser, S. Rotter, and K. Unterrainer, Random lasers for broadband directional emission, Optica **3**, 1035 (2016),

[108] P. W. Anderson, Absence of diffusion in certain random lattices, Phys. Rev. **109**, 1492 (1958).

[109] M. Lee, S. Callard, C. Seassal, and H.Jeon, Taming of random lasers, Nat. Photon. **13**, 445 (2019).

[110] C. Conti and A. Fratalocchi , Dynamic light diffusion, three-dimensional Anderson localization and lasing in inverted opals, Nat. Phys. **4**, 794. (2008).

[111] J. Liu, P. D. Garcia, S. Ek, N. Gregersen, T. Suhr, M. Schubert, J. Mørk, S. Stobbe, and P. Lodahl, Random nanolasing in the Anderson localized regime, Nat. Nanotechnol. **9**, 285 (2014).

[112] M. Gaio, D. Saxena, J. Bertolotti, D. Pisignano, A. Camposeo, and R. Sapienza A nanophotonic laser on a graph, Nat. Commun. **10**, 226 (2019).

[113] B. Kumar, R. Homri, Priyanka, S. K. Maurya, M. Lebental, and P. Sebbah, Localized modes revealed in random lasers, Optica **8**, 2334 (2021).

[114] S. P. Lau, H. Y. Yang, S. F. Yu, and H. D. Li, M. Tanemura, T. Okita, and H. Hatano, H. H. Hng, Laser action in ZnO nanoneedles selectively grown on silicon and plastic substrates, Appl. Phys. Lett. **87**, 013104 (2005).

[115] X. H. Wu, A.Yamilov, H. Noh, H. Cao, E. W. Seelig, and R. P. H. Chang, Random lasing in closely packed resonant scatterers. J. Opt. Soc. Am. B **21**,159 (2004).

[116] A. E. Siegmann, Lasers (University Science Books, Mill Valley, CA, 1986).

[117] M. A. Noginov, N. E. Noginova, H. J. Caulfield, P. Venkateswarlu, T. Thompson, M. Mahdi, and V. Ostroumov, Short-pulsed stimulated emission in the powders of $NdAl_3(BO_3)_4$, $NdSc_3(BO_3)_4$, and Nd:$Sr_5(PO_4)_3F$ laser crystals, J. Opt. Soc. Am. B **13**, 2024 (1996).

[118] M. A. Noginov, N. E. Noginova, S. U. Egarievwe, H. J. Caulfield, P. Venkateswarlu, A. Williams, and S. B. Mirov, Color-center powder laser: the effect of pulverization on color-center characteristics, J. Opt. Soc. Am. B **14**, 2153 (1997).

[119] T. Uchino and D. Okutsu, Broadband laser emission from color centers inside MgO microcrystals, Phys. Rev. Lett. **101**, 117401 (2008).

[120] T. Uchino, D. Okutsu, R. Katayama, and S. Sawai, Mechanism of stimulated optical emission from MgO microcrystals with color centers, Phys. Rev. B **79**, 165107 (2009).

[121] Y. Uenaka and T. Uchino, Photoexcitation, trapping, and recombination processes of the F-type centers in lasing MgO microcrystals, Phys. Rev. B **83**, 195108 (2011).

[122] V. M. Apalkov, M. E. Raikh, and B. Shapiro, Random resonators and prelocalized modes in disordered dielectric films, Phys. Rev. Lett. **89**, 016802 (2002).

[123] P. Sebbah and C. Vanneste, Random laser in the localized regime, Phys. Rev. B **66**, 144202 (2002).

[124] S. Mujumdar, M. Ricci, R. Torre, and D. S. Wiersma, Amplified extended modes in random lasers, Phys. Rev. Lett. **93**, 053903 (2004).

[125] S. Mujumdar, V. Türck, R.Torre, and D. S. Wiersma, Chaotic behavior of a random laser with static disorder, Phys. Rev. A **76**, 033807 (2007).

[126] C. Vanneste, P. Sebbah, and H. Cao, Lasing with resonant feedback in weakly scattering random systems, Phys. Rev. Lett. **98**, 143902 (2007).

[127] J. Andreasen, A. A. Asatryan, L. C. Botten, M. A. Byrne, H. Cao, L. Ge, L. Labonté, P. Sebbah, A. D. Stone, H. E. Türeci, and C. Vanneste, Modes of random lasers, Adv. Opt. Photonics **3**, 88 (2011).

[128] J. Fallert, R. J. B. Dietz, J. Sartor, D. Schneider, C. Klingshirn, and H. Kalt, Co-existence of strongly and weakly localized random laser modes. Nat. Photon. **3**, 279 (2009).

[129] Z. L. Wang, ZnO nanowire and nanobelt platform for nanotechnology, Mater. Sci. and Eng. R **64**, 33 (2009).

[130] S. Baruah and J. Dutta, Hydrothermal growth of ZnO nanostructures, Sci. Technol.

Adv. Mater. **10**, 013001 (2009).

[131] A. Kołodziejczak-Radzimska and T. Jesionowski, Zinc oxide—from synthesis to application: a review, Materials **7**, 2833 (2014).

[132] Z. L. Wang, Zinc oxide nanostructures: growth, properties and applications, J. Phys.: Condens. Matter **16**, R829 (2004).

[133] M. H. Huang, Y. Wu, H. Feick, N. Tran, E. Weber, P. Yang, Catalytic growth of zinc oxide nanowires by vapor transport, Adv. Mater. **13**, 113 (2001).

[134] Z. W. Pan , Z. R. Dai, and Z. L .Wang, Nanobelts of semiconducting oxides, Science **291**, 1947 (2001).

[135] S. H. Dalal, D. L. Baptista, K. B. K. Teo, R. G. Lacerda, D. A. Jefferson and W. I. Milne, Controllable growth of vertically aligned zinc oxide nanowires using vapour deposition, Nanotechnol. **17**, 4811 (2006).

[136] H.-Y. Li, S. Rühle, R. Khedoe, A. F. Koenderink, and D. Vanmaekelbergh, Polarization, microscopic origin, and mode structure of luminescence and lasing from single ZnO nanowires, Nano Lett. **9**, 3515 (2009).

[137] D. W. Bahnemann, C.. Kormann, and M. R. Hoffmann, Preparation and characterization of quantum size zinc oxide: a detailed spectroscopic study, J. Phys. Chem. **91**, 3789 (1987).

[138] A. van Dijken, E. A. Meulenkamp, D. Vanmaekelbergh, and A. Meijerink, Influence of adsorbed oxygen on the emission properties of nanocrystalline ZnO particles, J. Phys. Chem. B **104**, 18, 4355 (2000).

[139] G. Shi, C. M. Mo, W. L.Cai, and L. D. Zhang, Photoluminescence of ZnO nanoparticles in alumina membrane with ordered pore arrays, Solid State Commun. **115**, 253 (2000).

[140] M. Kohls, M. Bonanni, L. Spanhel, D. Su, and M. Giersig, Green Er^{III} luminescence in fractal ZnO nanolattices, Appl. Phys. Lett. **81**, 3858 (2002).

[141] Z. Qiu, K. S. Wong, M. Wu, W. Lin and H. Xu, Microcavity lasing behavior of oriented hexagonal ZnO nanowhiskers grown by hydrothermal oxidation, Appl. Phys. Lett. **84**, 2739 (2004).

[142] S. Baruah and J. Dutta, Hydrothermal growth of ZnO nanostructures, Sci. Technol. Adv. Mater. **10**, 013001 (2009).

[143] C. Xu, J. Dai, G. Zhu, G. Zhu, Y. Lin, J. Li, and Z. Shi, Whispering-gallery mode lasing in ZnO microcavities, Laser Photon. Rev. **8**, 469 (2014).

[144] H. Dong, B. Zhou, J. Li, J. Zhan, and L. Zhang, Ultraviolet lasing behavior in ZnO optical microcavities, J. Materiomics **3**, 255 (2017).

[145] K. J. Vahala, Optical microcavities, Nature **424**, 839 (2003)

[146] D. Saxena, S. Mokkapati, P. Parkinson, N. Jiang, Q. Gao, H. H. Tan and C. Jagadish, Optically pumped room-temperature GaAs nanowire lasers, Nat. Photon. **7**, 963 (2013).

[147] S. A. Church, R. A.-Abri, P. Parkinson, D. Saxena. Optical characterisation of nanowire lasers, Prog. Quantum Electron. **85**, 100408 (2022).

[148] Y. Ma, X. Guo, X. Wu, L. Dai, and L. Tong, Semiconductor nanowire lasers, Adv. Opt. Photon. **5**, 216 (2013).

[149] M. A Zimmler, F. Capasso, S. Müller and C.Ronning, Optically pumped nanowire lasers: invited review, Semicond. Sci. Technol. **25**, 02400 (2010).

[150] F. Vollmer and S. Arnold, Whispering-gallery-mode biosensing: label-free detection down to single molecules, Nat. Methods **5**, 591 (2008).

[151] V. S. Ilchenko, A. B. Matsko, Optical resonators with whispering-gallery modes-

part II: applications, IEEE J. Sel. Top. Quantum Electron. **12**, 15 (2006).

[152] A. Chiasera, Y. Dumeige, P. Féron, M. Ferrari, Y. Jestin, G. Nunzi Conti, S. Pelli, S. Soria, and G. C. Righini, Spherical whispering-gallery-mode microresonators, Laser Photon. Rev. **4**, 457 (2010).

[153] L. He, S. K. Özdemir, and L. Yang, Whispering gallery microcavity lasers, Laser Photon. Rev. **7**, 60 (2013).

[154] S, Yang, Y. Wang, and H. Sun, Advances and prospects for whispering gallery mode microcavities, Adv. Opt. Mater. **3**, 1136 (2015).

[155] Y. Chen, Y. Yin, L. Ma, and O.G. Schmidt, Recent progress on optoplasmonic whispering-gallery-mode microcavities, Adv. Opt. Mater. **9**, 2100143 (2021).

[156] J. C. Johnson, H. Yan, R. D. Schaller, L. H. Haber, R. J. Saykally, and P. Yang, Single nanowire lasers J. Phys. Chem. B **105**, 46, 11387 (2001)

[157] C. Johnson, H. Yan, P. Yang, and R. J. Saykally, Optical cavity effects in ZnO nanowire lasers and waveguides, J. Phys. Chem. B **107**, 34, 8816 (2003).

[158] A. V. Maslov and C. Z. Ning, Reflection of guided modes in a semiconductor nanowire laser, Appl. Phys. Lett. **83**, 1237 (2003).

[159] J. P. Richters, J. Kalden, M. Gnauck, C. Ronning, C. P. Dietrich, H. von Wenckstern, M. Grundmann, J. Gutowski and T. Voss, Modal gain and its diameter dependence in single-ZnO micro- and nanowires, Semicond. Sci. Technol. **27** 015005 (2012).

[160] K. L. Shaklee and R. F. Leheny, Direct determination of optical gain in semiconductor crystals, Appl. Phys. Lett. 18, 475 (1971).

[161] K. L. Shaklee, R. E. Nahory, R. F. Leheny, Optical gain in semiconductors, J. Lumin. **7**, 284 (1973).

[162] P. L. Knight and A. Miller, Vertical-cavity surface emitting laser (Springer-Verlag,

Berlin, 1999).

[163] H. Yan, J. Johnson, M. Law, R. He, K. Knutsen, J. R. McKinney, J. Pham, R. Saykally, and P. Yang, ZnO Nanoribbon microcavity lasers, Adv. Mater. **15**, 1907 (2003).

[164] B. Zou, R. Liu, F. Wang, A. Pan, L. Cao, and Z. L. Wang, Lasing mechanism of ZnO nanowires/nanobelts at room temperature, J. Phys. Chem. B **110**, 26, 12865 (2006).

[165] J. M. Szarko, J. K. Song, C. W. Blackledge, I. Swart, S. R. Leone, S. Li, and Y. Zhao, Optical injection probing of single ZnO tetrapod lasers, Chem. Phys. Lett. **404**, 171 (2005).

[166] M. A. Zimmler, J. Bao, F. Capasso, S. Müller, and C. Ronning, Laser action in nanowires: Observation of the transition from amplified spontaneous emission to laser oscillation, Appl. Phys. Lett. **93**, 051101 (2008).

[167] A. E. Siegman, Lasers (University Science Books, Sausalito, 1986).

[168] T. P. H. Sidiropoulos, R. Röder, S. Geburt, O. Hess, S. A. Maier, C. Ronning, and R. F. Oulton, Ultrafast plasmonic nanowire lasers near the surface plasmon frequency, Nat. Phys. **10**, 870 (2014)

[169] J. Lu, M. Jiang, M. Wei, C. Xu, S, Wang, Z. Zhu, F. Qin, Z, Shi, and C. Pan, Plasmon-induced accelerated exciton recombination dynamics in ZnO/Ag hybrid nanolasers, ACS Photonics **4**, 2419 (2017).

[170] Y.-J. Lu, J. Kim, H.-Y. Chen, C. Wu, N.Dabidian, C. E Sanders, C.-Y. Wang, M.-Y. Lu, B.-H. Li, X. Qiu, W.-H. Chang, L.-J. Chen, G. Shvets, C.-K. Shih, and S. Gwo, Plasmonic nanolaser using epitaxially grown silver film, Science **337**, 450 (2012).

[171] J. Li, M. Jiang, C. Xu, Y. Wang, Y. Lin, J. Lu, and Z. Shi, Plasmon coupled Fabry-Perot lasing enhancement in graphene/ZnO hybrid microcavity, Sci. Rep. **5**, 9263 (2015).

[172] Y.-H. Chou, K.-B. Hong, C.-T. Chang, T.-C. Chang, Z.-T. Huang, P.-J. Cheng, J.-H. Yang, M.-H. Lin, T.-R. Lin, K.-P. Chen, S. Gwo, and T.-C. Lu, Ultracompact pseudowedge plasmonic lasers and laser arrays, Nano Lett. **18**, 2, 747 (2018).

[173] S. Chu, G. Wang, W. Zhou, Y. Lin, L. Chernyak, J. Zhao, J. Kong, L. Li, J. Ren, and J. Liu, Electrically pumped waveguide lasing from ZnO nanowires, Nat. Nanotechnol. **6**, 506 (2011).

[174] J. Y. Zhang, Q. F. Zhang, T. S. Deng, and J. L. Wu, Electrically driven ultraviolet lasing behavior from phosphorus-doped pZnO nanonail array/n-Si heterojunction Appl. Phys. Lett. **95**, 211107 (2009).

[175] X. Duan, Y. Huang, R. Agarwal, and C. M. Lieber, Single nanowire electrically driven lasers, Nature **421**, 241 (2003).

[176] K. H. Li, X. Liu, Q. Wang, S. Zhao, and Z. Mi , Ultralowthreshold electrically injected AlGaN nanowire ultraviolet lasers on Si operating at low temperature, Nat. Nanotechnol. **10**, 140 (2015).

[177] S. Zhao, S. Y. Woo, M. Bugnet, X. Liu, J. Kang, G. A. Botton, and Z. Mi, Three-dimensional quantum confinement of charge carriers in self-organized AlGaN nanowires: A viable route to electrically injected deep ultraviolet lasers, Nano Lett. **15**, 7801 (2015).

[178] J. Wiersig, Hexagonal dielectric resonators and microcrystal lasers, Phys. Rev. A **67**, 023807 (2003).

[179] C. P. Dietrich, M. Lange, T. Böntgen, and M. Grundmann, The corner effect in

hexagonal whispering gallery microresonators, Appl. Phys. Lett. **101**, 141116 (2012).

[180] J. Dai, C. X. Xu, K. Zheng, C. G. Lv, and Y. P. Cui, Whispering gallery-mode lasing in ZnO microrods at room temperature, Appl. Phys. Lett. **95**, 241110 (2009).

[181] R. Chen, B. Ling, X. Wei Sun, and H. D. Sun, Room temperature excitonic whispering gallery mode lasing from high-quality hexagonal ZnO microdisks, Adv. Mater. **23**, 2199 (2011).

[182] J. Dai, C. X. Xu, P. Wu, J. Y. Guo, Z. H. Li, and Z. L. Shi, Exciton and electron-hole plasma lasing in ZnO dodecagonal whispering-gallery-mode microcavities at room temperature, Appl. Phys. Lett. **97**, 011101 (2010).

[183] J. Dai, C. X. Xu, and X. W. Sun, ZnO-microrod/p-GaN heterostructured whispering-gallery-mode microlaser diodes, Adv. Mater. **23**, 4115 (2011).

[184] Q. Zhang, J. Qi, X. Li, F. Yi, Z. Wang, and Y. Zhang, Electrically pumped lasing from single ZnO micro/nanowire and poly(3,4-ethylenedioxythiophene): poly(styrenexulfonate) hybrid heterostructures, Appl. Phys. Lett. **101**, 043119 (2012).

[185] X. Zhou, M. Jiang, K. Xu, M. Liu, S. Sha, S.n Cao, C. Kan, and D. N, Shi, Electrically driven single microwire-based single-mode microlaser, Light: Sci. Appl. **11**, 198 (2022).

[186] C. F. Klingshirn, Semiconductor Optics, 2nd ed. (Springer, Berlin, 2005).

[187] F. Sekiguchi, T. Mochizuki, C. Kim, H. Akiyama, L. N. Pfeiffer, K. W. West, and R.Shimano, Anomalous metal phase emergent on the verge of an exciton Mott transition, Phys. Rev. Lett. **118**, 067401(2017).

[188] C. Klingshirn, R. Hauschild, J. Fallert, and H. Kalt, Room-temperature stimulated

emission of ZnO: Alternatives to excitonic lasing, Phys. Rev. B **75**, 115203 (2007).

189 M. A. M. Versteegh, T. Kuis, H. T. C. Stoof, and J. I. Dijkhuis, Ultrafast screening and carrier dynamics in ZnO: Theory and experiment, Phys. Rev. B **84**, 035207 (2011).

190 M. A. M. Versteegh, D. Vanmaekelbergh, and J. I. Dijkhuis, Room-temperature laser emission of ZnO nanowires explained by many-body theory, Phys. Rev. Lett. **108**, 157402 (2012).

191 E. Hendry, M. Koeberg, and M. Bonn, Exciton and electron-hole plasma formation dynamics in ZnO, Phys. Rev. B **76**, 045214 (2007).

192 A. Schleife, C. Rödl, F. Fuchs, K. Hannewald, and F. Bechstedt, Optical absorption in degenerately doped semiconductors: Mott transition or Mahan excitons? Phys. Rev. Lett. **107**, 236405 (2011).

193 M. Wille, C. Sturm, T. Michalsky, R. Röder, C. Ronning, R. Schmidt-Grund and M. Grundmann, Carrier density driven lasing dynamics in ZnO nanowires, Nanotechnol. **27**, 225702 (2016).

194 C. B. à la Guillaume, J.-M. Debever, and F. Salvan, Radiative recombination in highly excited CdS, Phys. Rev. **177**, 567 (1969).

195 M. Hvam, Exciton-exciton interaction and laser emission in high-purity ZnO, Solid. State Commun. **12**, 95 (1973).

196 M. Hvam, Exciton interaction in photoluminescence from ZnO, Phys. Stat. Sol. B, **63**, 511 (1974).

197 C. Klingshirn, The luminescence of ZnO under high one- and two-quantum excitation, Phys. Stat. Sol. B **71**, 547 (1975).

198 B. Hönerlage,C. Klingshirn, and J. B. Grun, Spontaneous emission due to exciton-

electron scattering in semiconductors, Phys. Stat. Sol. B **78**, 599 (1976).

[199] H. Haug and S. Koch, On the theory of laser action in dense exciton systems, Phys. Stat. Sol. B **82**, 531 (1977).

[200] C. Klingshirn and H. Haug, Optical properties of highly excited direct gap semiconductors, Phys. Rep. **70**, 315 (1981).

[201] I. Pelant and J. Valenta, Luminescence Spectroscopy of Semiconductors (Oxford University Press, Oxford, 2012).

[202] H. Priller, J. Brückner, Th. Gruber, C. Klingshirn, H. Kalt, A. Waag, H. J. Ko, T. Yao, Comparison of linear and nonlinear optical spectra of various ZnO epitaxial layers and of bulk material obtained by different experimental techniques, Phys. Stat. Sol. B **241**, 587 (2004).

[203] R. Matsuzaki, H.Soma, K. Fukuoka, K. Kodama, A. Asahara, T. Suemoto, Y. Adachi, and T. Uchino, Purely excitonic lasing in ZnO microcrystals: Temperature-induced transition between exciton-exciton and exciton-electron scattering, Phys. Rev. B **96**, 125306 (2017).

[204] S. Fujii, Y. Adachi, and T. Uchino, Excitonic stimulated emission from $Mg_xZn_{1-x}O$ films due to enhanced exciton binding energy, Phys. Rev. B **102**, 075204 (2020).

[205] B. E. Sernelius, K.-F. Berggren, Z.-C. Jin, I. Hamberg, and C. G. Granqvist, Band-gap tailoring of ZnO by means of heavy Al doping, Phys. Rev. B **37**, 10244 (1988).

[206] S. C. Jain, J. M. McGregor, and D. J. Roulston, Band-gap narrowing in novel III-V semiconductors, J Appl. Phys. **68**, 3747 (1990).

[207] J. A. Sans, J. F. Sánchez-Royo, A. Segura, G. Tobias, and E. Canadell, Chemical effects on the optical band-gap of heavily doped ZnO:M_{III}(M=Al,Ga,In): An investigation by means of photoelectron spectroscopy, optical measurements under

pressure, and band structure calculations, Phys. Rev. B **79**, 195105 (2009).

[208] E. Burstein, Anomalous Optical Absorption Limit in InSb, Phys. Rev. **93**, 632 (1954).

[209] T. S. Moss, Optical Properties of Semiconductors (Butterworths, London, 1961).

[210] G. D. Mahan, Excitons in Degenerate Semiconductors, Phys. Rev. **153**, 882 (1967).

[211] F. Fuchs, K. Kheng, P. Koidl, and K. Schwarz, Fermi-edge singularity in degenerate n-type bulk InAs, Phys. Rev. B **48**, 7884 (1993).

[212] M. Feneberg, J. Däubler, K. Thonke, R. Sauer, P. Schley, and R. Goldhahn, Mahan excitons in degenerate wurtzite InN: Photoluminescence spectroscopy and reflectivity measurements, Phys. Rev. B **77**, 245207 (2008).

[213] P. Plochocka-Polack, J. G. Groshaus, M. Rappaport, V. Umansky, Y. Gallais, A. Pinczuk, and I. Bar-Joseph, Fermi-Edge Singularity of Spin-Polarized Electrons, Phys. Rev. Lett. **98**, 186810 (2007).

[214] T. Palmieri, E. Baldini, A. Steinhoff, A. Akrap, M. Kollár, E. Horváth, L. Forró, F. Jahnke, and M. Chergui , Mahan excitons in room-temperature methylammonium lead bromide perovskites, Nat. Commun. **11**, 850 (2020).

[215] S. Richter, O. Herrfurth, S. Espinoza, M. Rebarz, M. Kloz, J. A Leveillee, A. Schleife, S. Zollner, M.Grundmann, J. Andreasson, and R. Schmidt-Grund, Ultrafast dynamics of hot charge carriers in an oxide semiconductor probed by femtosecond spectroscopic ellipsometry, New J. Phys. **22**, (2020).

[216] T. Nakamura, K. Firdaus, and S. Adachi, Electron-hole plasma lasing in a ZnO random laser, Phys. Rev. B **86**, 205103 (2012).

[217] J. C. Johnson, K. P. Knutsen, H. Yan, M. Law, Y. Zhang, P. Yang, and R. J. Saykally Ultrafast carrier dynamics in single ZnO nanowire and nanoribbon Lasers, Nano

Lett. **4**, 197 (2004).

[218] A, B. Djurišić, W. M. Kwok, Y. H. Leung, D. L. Phillips, and W. K. Chan, Stimulated emission in ZnO nanostructures: A rime-resolved study, J. Phys. Chem. B **109**, 19228 (2005).

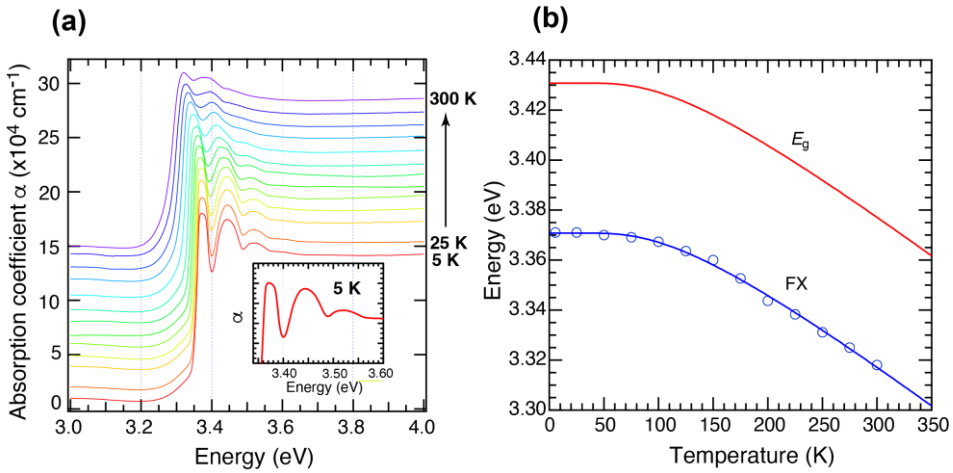

FIG. 1. (a) Absorption coefficient spectra for a 249-nm thick ZnO film measured at different temperatures from 5 to 300 K. In the temperature range from 25 to 300 K, spectra are shown in steps of 25 K. The inset shows a magnified view of the spectrum at 5 K. (b) Temperature dependent change in the free exciton (FX) peak (blue open circles). The blue solid line represents the fit to Eq. (2). The red solid line is the temperature dependence of the band gap E_g expected from Eq. (2) and $E_X^b = 60$ meV

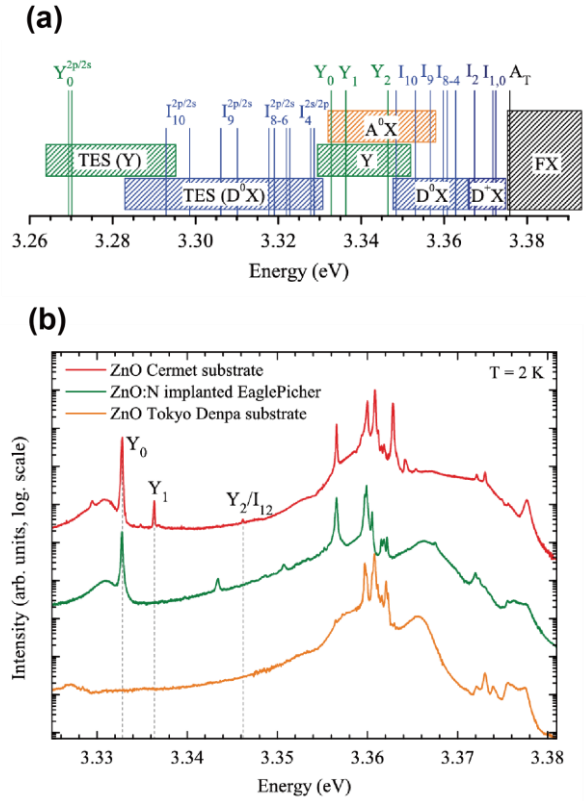

FIG. 2. (a) Schematic drawing of the energy ranges of various optical transitions of ZnO at low temperature. Selected transitions are indicated by vertical lines. The different areas mark the energy range of free excitons (FX), ionized donor bound excitons (D^+X), neutral donor bound excitons (D^0X), acceptor bound excitons (A^0X), deeply bound excitons (Y), and two electron satellites (TES) of shallow and deeply bound excitons in their 2s and 2p states. (b) PL spectra of different ZnO crystals at T=2K. Several narrow emission lines are visible in the spectral range 3.33 and 3.35 eV. The strongest peaks are the Y_0 and the Y_1 lines. The spectra are vertically shifted and normalized to the dominant bound exciton line. Reproduced with permission from M. R. Wagner *et al.*, Phys. Rev. B **84**, 035313 (2011). Copyright 2011 the American Physical Society.

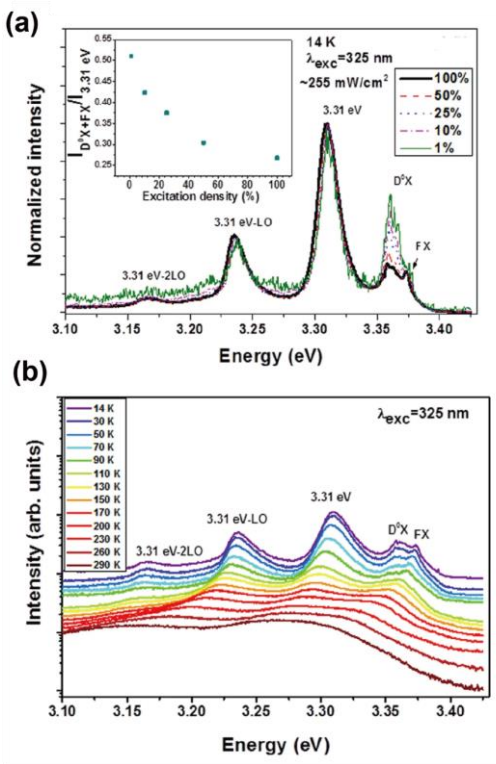

FIG. 3. (a) Excitation density dependence of the near band edge emission of the ZnO microrods recorded at 14 K. The inset depicts the ratio between the $D^0X + FX$ and 3.31 eV emission intensity as a function of excitation power. (b) Temperature dependence of the near band edge emission. Reproduced with permission from J. Rodrigues *et al.*, Sci. Rep. **5**, 10783 (2015). Copyright 2015 Springer Nature.

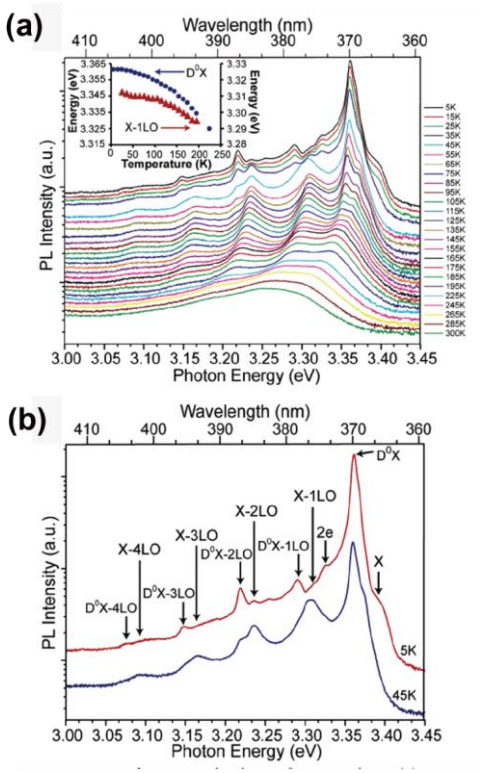

FIG. 4. (a) Log plot of the band edge emission of a single ZnO nanowire as a function of temperature (pump power ~50 Wcm^{-2}). The inset plots the donor bound (D^0X) and first-order free-exciton phonon replica (X-1LO) peaks as a function of temperature. (b) Zoom in of the 5 and 45 K spectra showing the excitonic fine structure. Reproduced with permission from D. J. Sirbuly *et al.*, J. Phys. Chem. B **109**, 32, 15213 (2005). Copyright 2005 American Chemical Society.

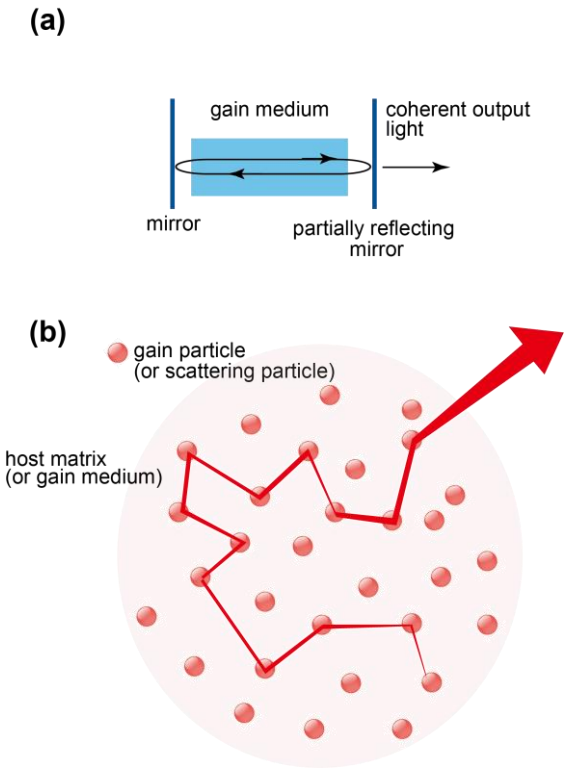

FIG. 5. Schematic illustration of two different feedback mechanisms: (a) a conventional Fabry-Perot resonator, (b) a random laser cavity.

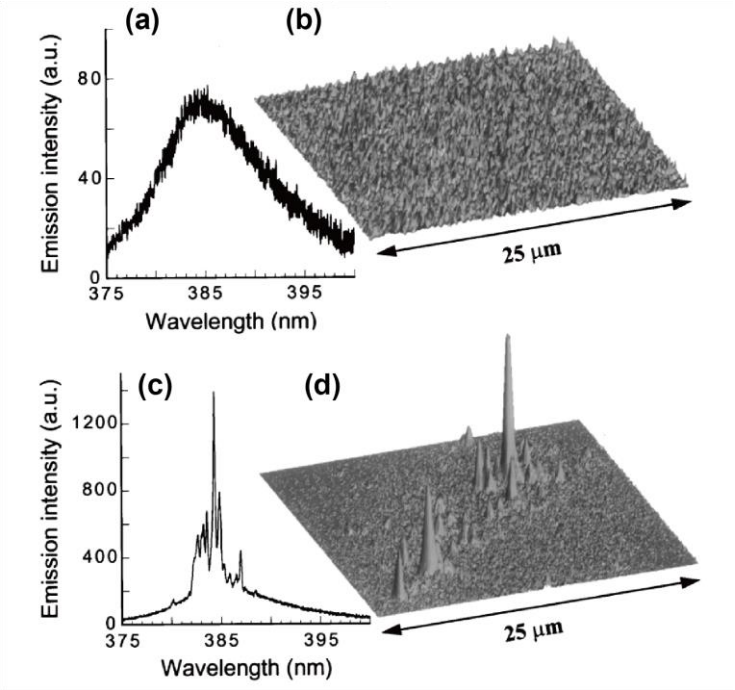

FIG. 6. Random laser action from a ZnO powder film at different pump power. (a), (c) the measured spectra of emission. (b), (d) the measured spatial distribution of emission intensity in the film. The incident pump pulse energy is 5.2 nJ for (a) and (b), and 12.5 nJ for (c) and (d). Reproduced with permission from H. Cao *et al.*, Phys. Rev. Lett. **84**, 5584 (2000).. Copyright 2000 the American Physical Society.

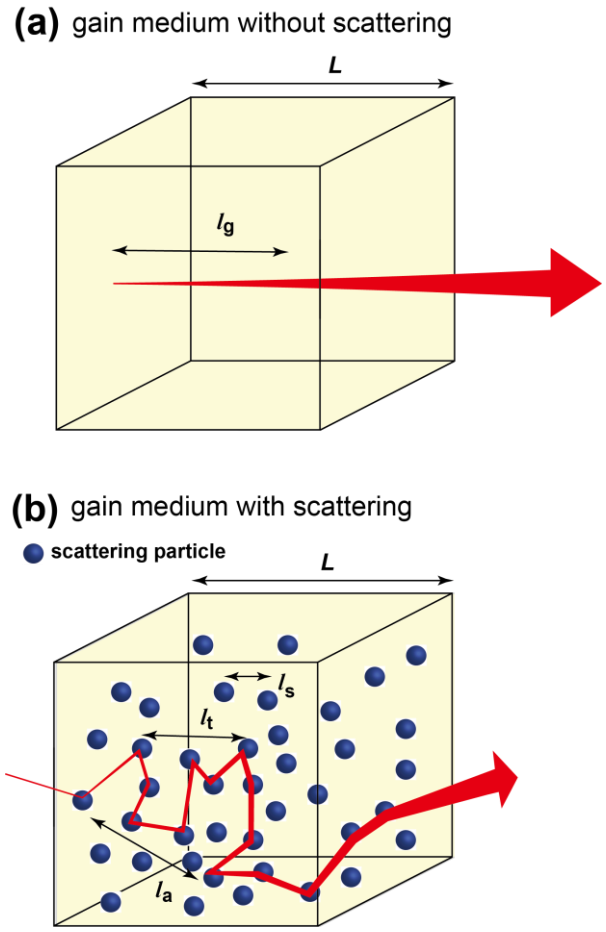

FIG. 7. Light propagation in a three-dimensional gain medium with length of L (a) without and (b) with scattering. In (a), gain length l_g is defined as a distance that optical signal has to travel to achieve amplification by a factor of $e \approx 2.72$. In (b), scattering mean free path l_s, transport mean free path l_t, and amplification length l_a are schematically shown.

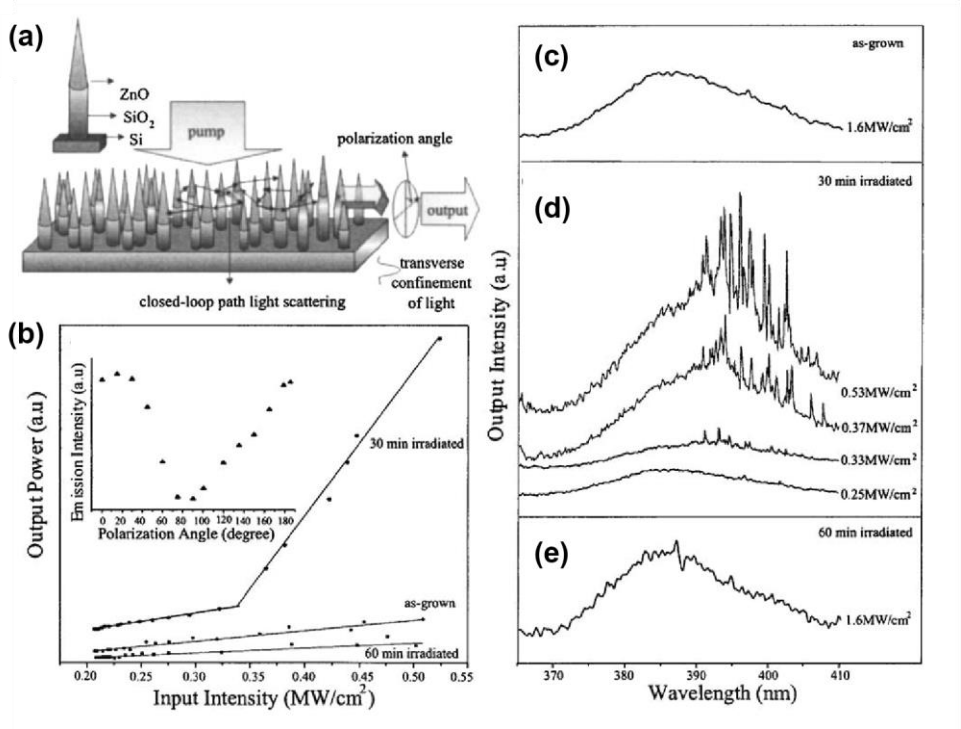

FIG. 8. (a) Schematic diagram of the laser measurement setup for the ZnO nanoneedle arrays. (b) Light-light curves of the samples after various ion irradiation times. The inset shows the maximum emission intensity of the TE mode as a function of polarization angles. (c) Emission spectrum of the as-grown ZnO thin film under pump power of 1.6 $MWcm^{-2}$. (d) Evolution of emission spectra of the 30-min irradiated sample under different pump intensities. (e) Emission spectrum of the sample irradiated for 60min under pump power of 1.6 $MWcm^{-2}$. Reproduced with permission from S. P. Lau *et al.*, Appl. Phys. Lett. 87, 013104 (2005). Copyright 2005 AIP Publishing.

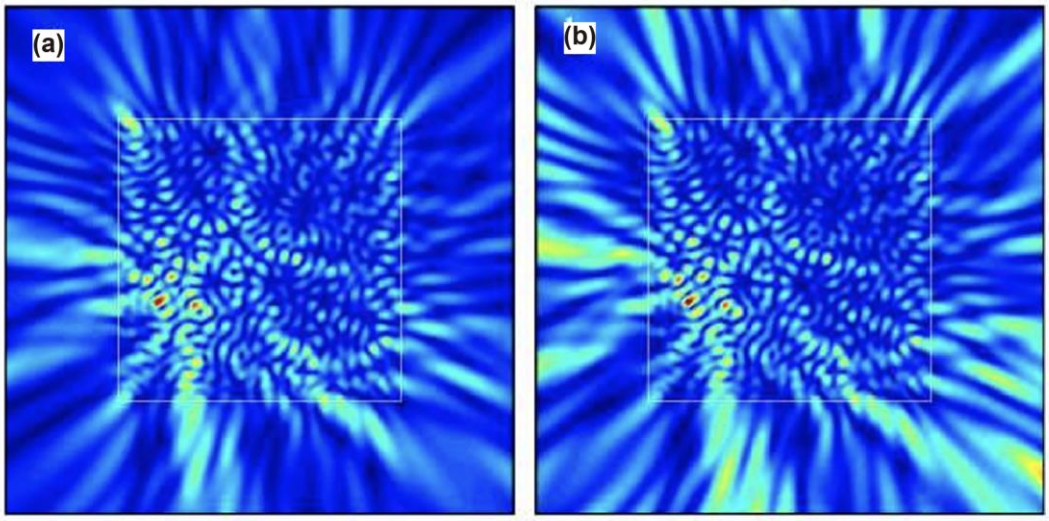

FIG. 9. (a) Spatial distribution of the amplitude of a lasing mode in the diffusive regime. (b) Spatial distribution of the field amplitude after the pump has been stopped and the polarization term has been set to zero. The system consists of 896 circular scatterers contained in a square box of size L=5 μm and optical index n=1.The radius r and n of the scatterers are r = 60 nm and n = 1.25, respectively, Reproduced with permission from J. Andreasen *et al.*, Adv. Opt. Photonics **3**, 88 (2011). Copyright 2011 Optical Society of America.

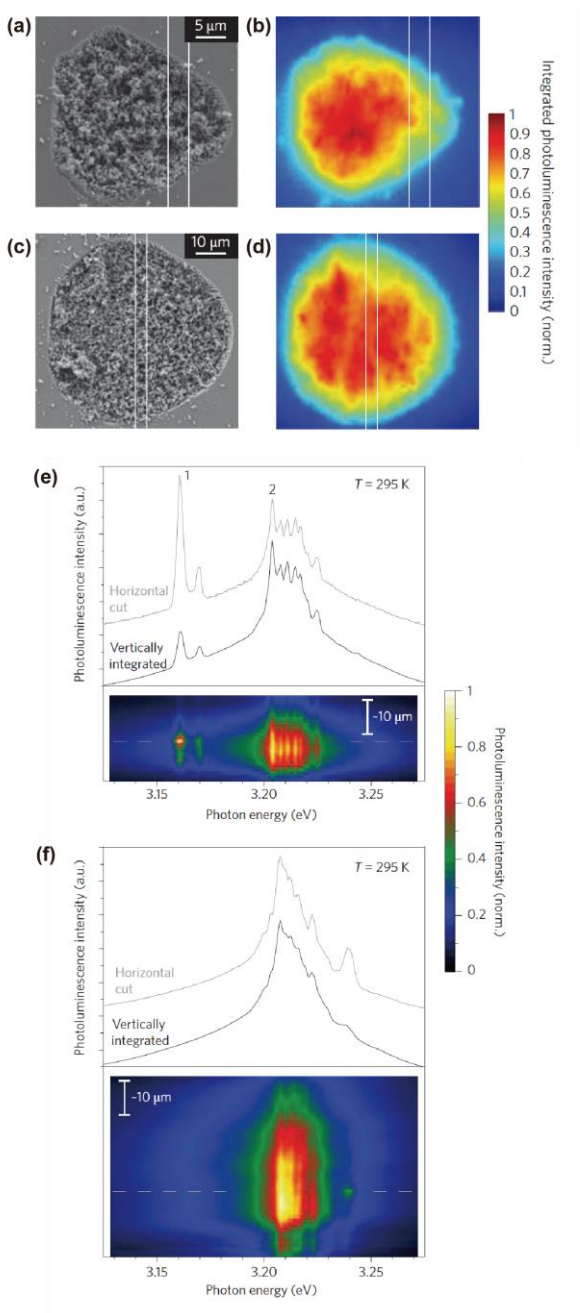

FIG. 10. (a),(c) SEM images of two structured fields of ZnO nanoparticles with a mean particle size of 260 nm. (b),(d) Spatially resolved total photoluminescence of the respective fields at room temperature and an excitation density of 2.5 MW cm^{-2}. (e),(f) The spectrally resolved photoluminescence taken from a vertically extended and horizontally limited (to 3.5 µm) spatial region. The area between the white lines in (a) and (c) indicates the area from which the photoluminescence of panels (e) and (f) is taken. Reproduced with permission from J. Fallert *et al.*, Nat. Photon. **3**, 279 (2009). Copyright 2009 Springer Nature.

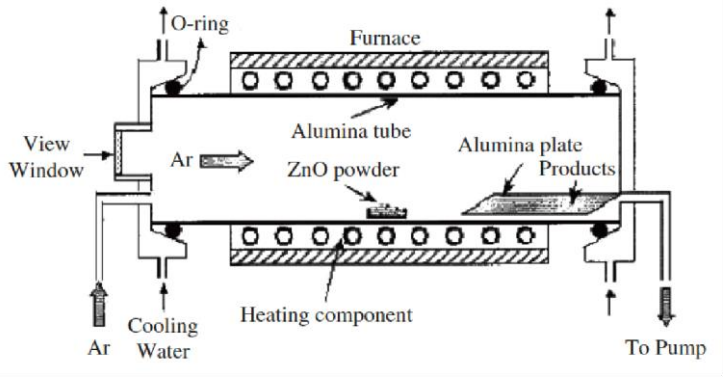

FIG. 11. A schematic diagram of the experimental apparatus for growth of oxides nanostructures by the vapor-liquid-solid (VLS) growth method. Reproduced with permission from Z. L. Wang, J. Phys.: Condens. Matter **16**, R829 (2004). Copyright 2004 IOP Publishing.

.

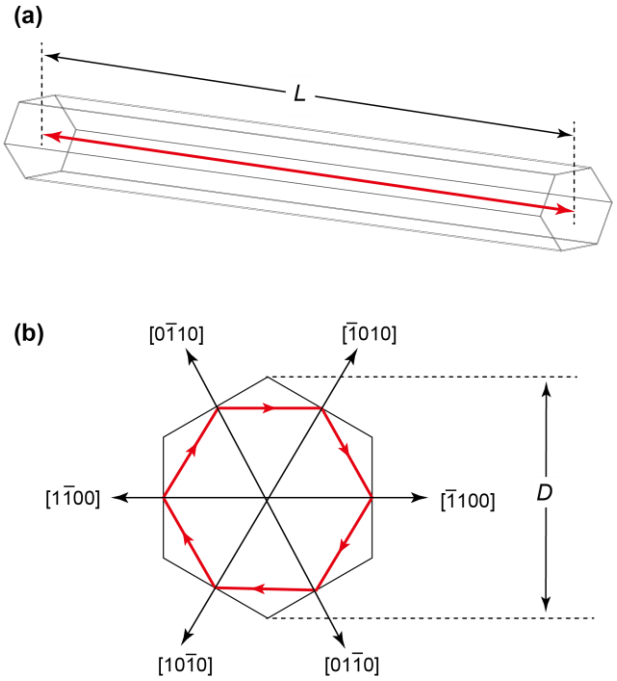

FIG. 12. Schematic illustration of (a) a Fabry-Perot nanowire cavity and (b) a hexagonal whispering gallery mode cavity.

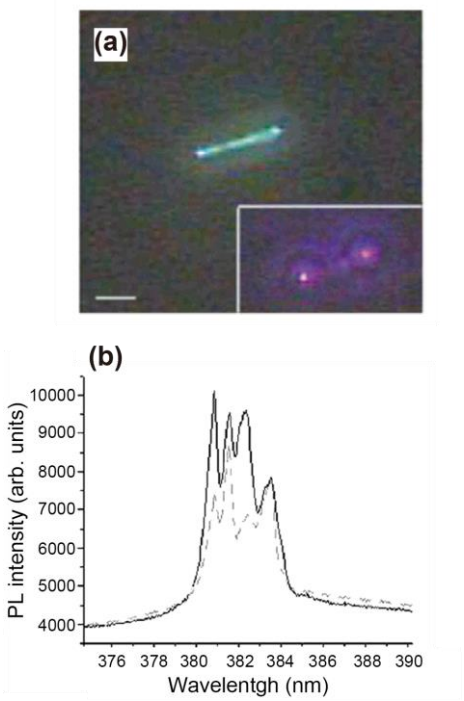

FIG. 13. (a) Far-field image and (b) PL spectrum of an individual ZnO nanowire under unpolarized continuous wave excitation at 325 nm. Inset: UV-stimulated emission image of the nanowire with pulsed excitation. Reproduced with permission from C. Johnson *et al.*, J. Phys. Chem. B 107, **34**, 8816 (2003). Copyright 2003 American Chemical Society.

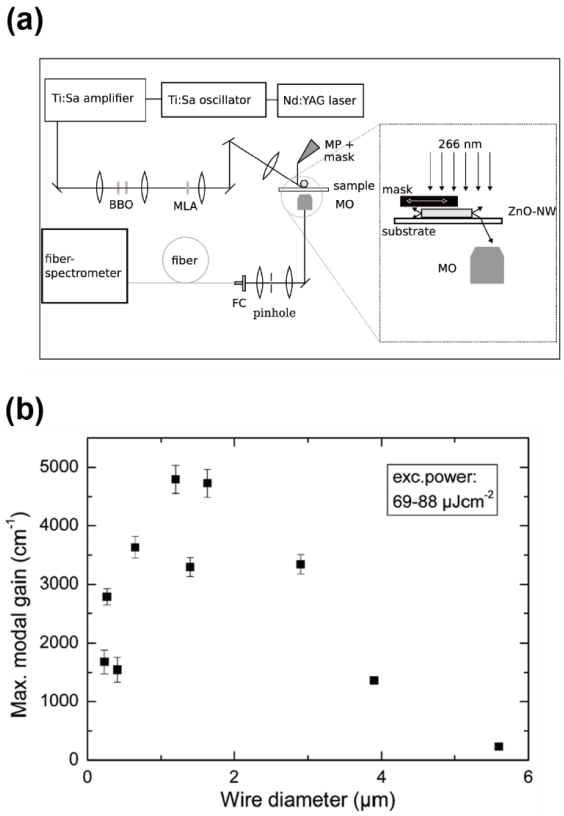

FIG. 14. (a) Schematic plot of the experimental setup. 266 nm fs laser pulses are used to excite the nanowire. A mask is used to define the excited length of the nanowire (details in the inset). (b) Maximum values of the modal gain in dependence on the nanowire diameter at an excitation density of 69–88 μJcm^{-2}. Reproduced with permission from J. P. Richters *et al.*, Semicond. Sci. Technol. **27**, 015005 (2012). Copyright 2012 IOP Publishing.

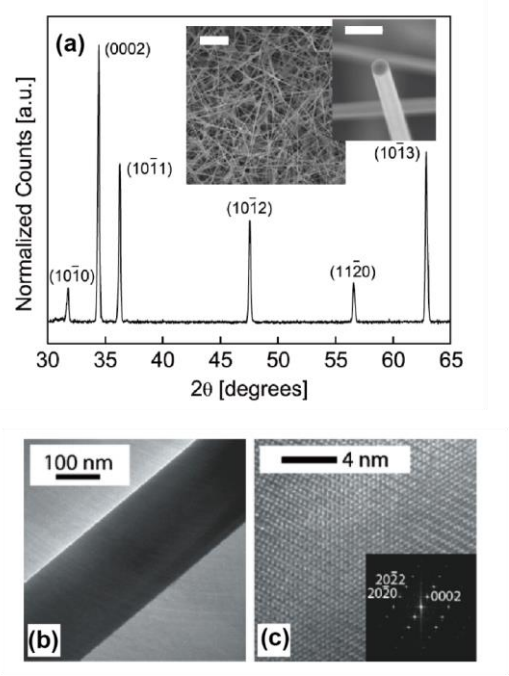

FIG. 15. (a) Representative X-diffraction pattern of an as-grown ZnO nanowire ensemble sample. Inset (left): SEM micrograph of the as-grown ensemble of ZnO nanowires on the growth substrate. The scale bar is 10 μm. Inset (right): SEM micrograph of a single ZnO nanowire. The scale bar is 500 nm. (b) Bright-field and (c) high-resolution TEM micrographs of an individual ZnO nanowire. Inset: FFT analysis of (c). Reproduced with permission from M. A Zimmler *et al*., Semicond. Sci. Technol. **25**, 02400 (2010). Copyright 2010 IOP Publishing.

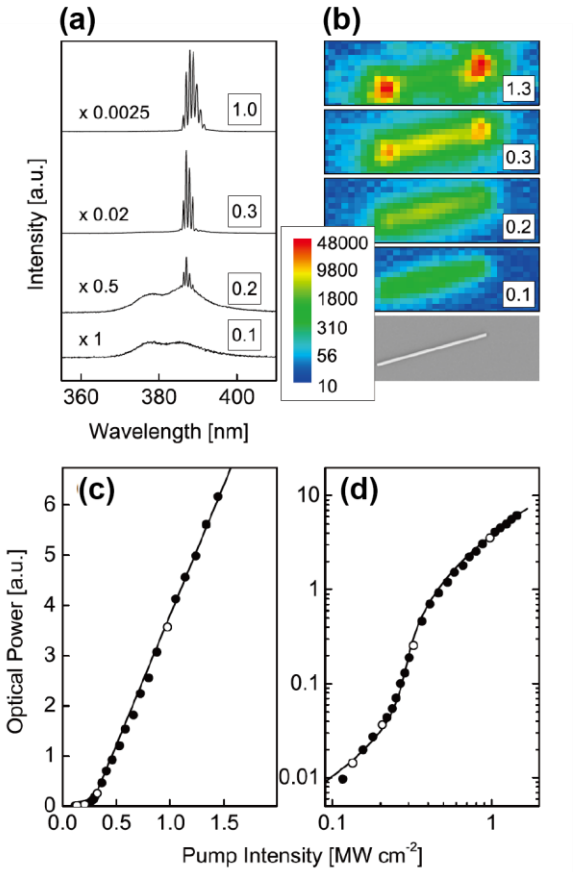

FIG. 16. Laser oscillation in ZnO nanowires. (a) Output spectra versus pump intensity of a 12.2 μm long 250 nm diameter ZnO nanowire. (b) SEM image and CCD images, under different pump intensities, for the same nanowire as in (a). The labels indicate the pump intensity in units of MW cm^{-2}. The color scale indicates the number of counts. (c) Pump intensity dependence of the total output power (circles) for the same nanowire. The optical power was collected from the scattered light at one of the nanowire ends. (d) The same data and fit on a log–log scale. The open circles correspond to the spectra shown in (a). Reproduced with permission from M. A Zimmler *et al.*, Semicond. Sci. Technol. **25**, 02400 (2010). Copyright 2010 IOP Publishing.

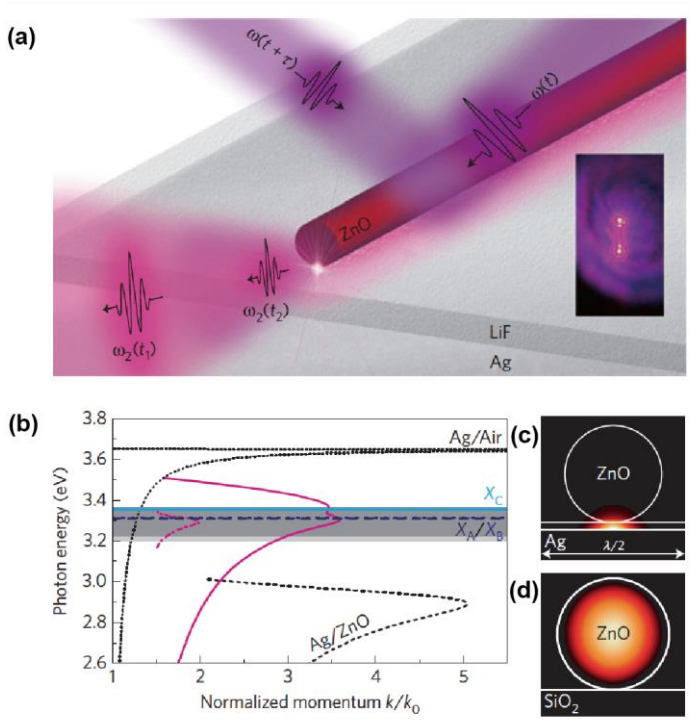

FIG. 17. (a) Schematic of the geometry and the emission of a ZnO nanowire optically excited with two time-delayed (τ) pump pulses. The inset shows a picture of a lasing plasmonic nanowire. (b) Calculated dispersion relation for various metallic interfaces plotted as photon energy versus normalized momentum (k/k_0). The different curves are for a silver–air interface (black dotted line), silver–ZnO interface (black dashed line), a 150 nm diameter ZnO wire on SiO_2 (pink dash-dotted line) without cutoff $k/k_0 < 1.5$, and a 130 nm diameter ZnO wire close to a silver surface (pink solid line). The three ZnO exciton lines are labelled with XA, XB, XC and the overlapping shaded areas indicate the electron–hole plasma gain region (light grey) and plasmonic laser emission region (dark grey). (c),(d) Calculated nanowire modes for a 130 nm diameter ZnO wire on a Ag/LiF (100/10 nm) interface and a 150 nm diameter ZnO wire on a SiO_2 substrate, respectively. Reproduced with permission from T. P. H. Sidiropoulos *et al*., Nat. Phys. **10**, 870 (2014). Copyright 2014 Springer Nature.

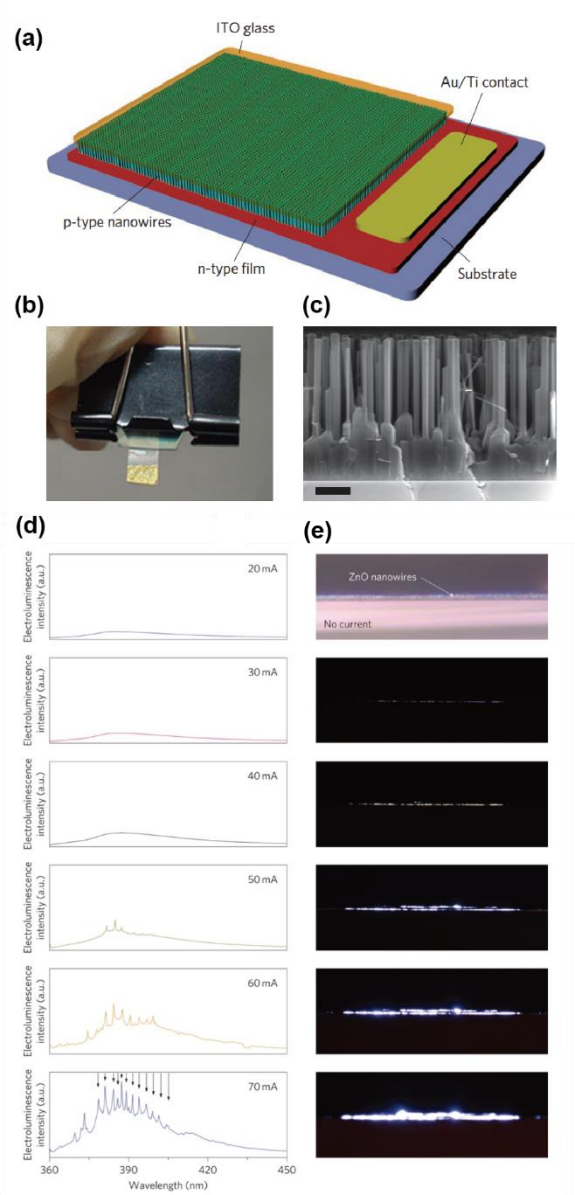

FIG. 18. (a) Schematic of the laser device, which consists of an n-type ZnO thin film on a c-sapphire substrate, p-type vertically aligned ZnO nanowires, ITO contact and Au/Ti contact. (b) Photo-image of the device. (c) Side-view SEM image of the device structure showing the ZnO thin film and nanowires. Scale bar, 1 μm. (d) Electroluminescence spectra of the laser device operated between 20 mA and 70 mA. Above 50 mA, lasing characteristics are clearly observed. Arrows in the 70 mA spectrum represent quasi-equidistant peaks. (e) Side-view optical microscope images of the lasing device, corresponding to the electroluminescence spectra in (d) The first image was taken with lamp illumination and without current injection. Reproduced with permission from S. Chu *et al*., Nat. Nanotechnol. **6**, 506 (2011). Copyright 2011 Springer Nature.

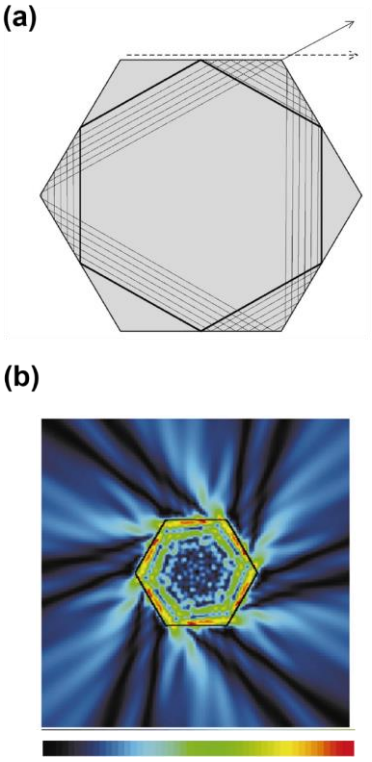

FIG. 19. (a) Semiclassical ray model of a hexagonal dielectric resonator. Thick line marks a member of the family of long-lived rays, other members are obtained by shifting the ray along the boundary (not shown). The thin line marks a ray with slightly different angle of incidence. Arrows indicate emission due to pseudointegrable dynamics (thin) and boundary waves (dashed). (b) An example of calculated near field intensity pattern. Reproduced with permission from J. Wiersig, Phys. Rev. A **67**, 023807 (2003). Copyright 2003 the American Physical Society.

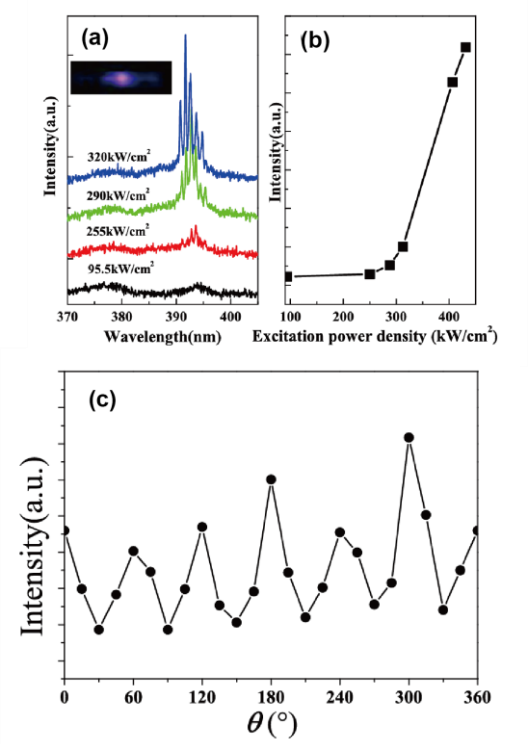

FIG. 20. (a) Emission spectra of the ZnO microrod (D=6.67 μm) excited by a Nd:YAG laser with different excitation power density. The inset is the far-field image of the lasing ZnO microrod taken by a digital camera. (b) The relationship between output lasing. (c) The far-field lasing intensity distribution around the c-axis of the hexagonal ZnO microrod with the diagonal of 6.67 μm. Reproduced with permission from J. Dai *et al.*, Appl. Phys. Lett. **95**, 241110 (2009). Copyright 2009 AIP Publishing.

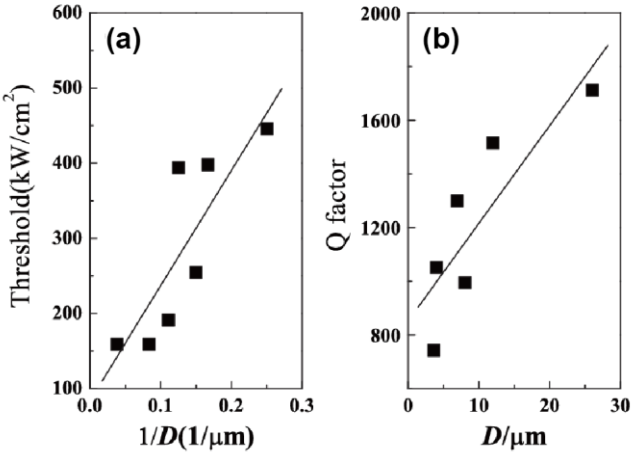

FIG. 21. The dependence of (a) the lasing threshold and (b) the Q factor on the diagonal of the hexagonal ZnO microrods. Reproduced with permission from J. Dai *et al.*, Appl. Phys. Lett. **95**, 241110 (2009). Copyright 2009 AIP Publishing.

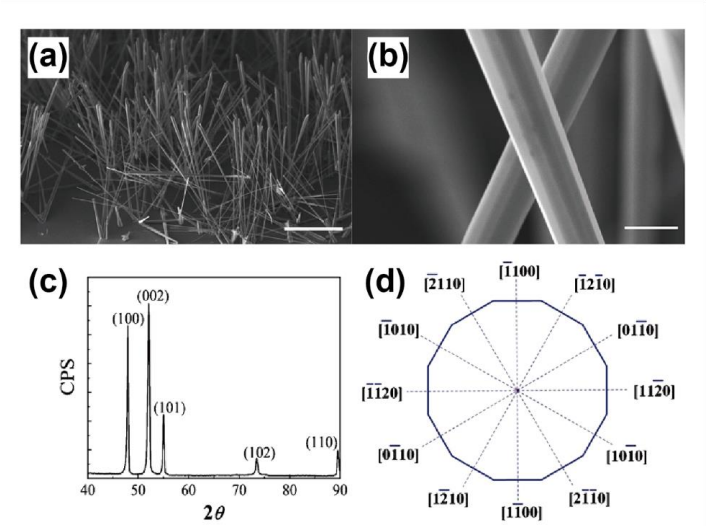

FIG. 22. (a) SEM image of the size view of ZnO dodecagonal microrods (the substrate is 60° tilted to the sample platform), the scale bar is 200 μm. (b) The enlarged SEM image of the microrods with higher magnification, the scale bar is 5 μm. (c) XRD pattern for the bulk of ZnO dodecagonal microrods. (d) 12 crystal facets for dodecagonal microrods. Reproduced with permission from J. Dai *et al.*, Appl. Phys. Lett. **97**, 011101 (2010). Copyright 2010 AIP Publishing.

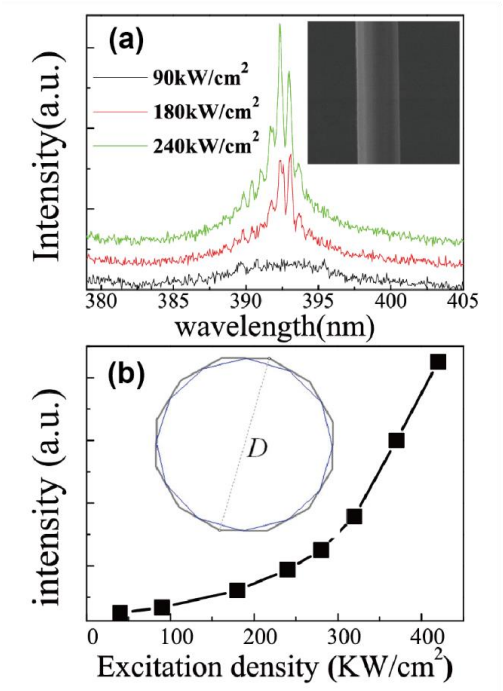

FIG. 23. (a) Exciton lasing mission spectra of the ZnO microwire (D=6.35 μm) excited by a Nd:YAG laser with different excitation power density. The inset shows the SEM image of the selected dodecagonal microrod. (b) The relationship between output lasing intensity and excitation power density. The inset shows the WGM optical path in the dodecagonal cavity. Reproduced with permission from J. Dai *et al.*, Appl. Phys. Lett. **97**, 011101 (2010). Copyright 2010 AIP Publishing.

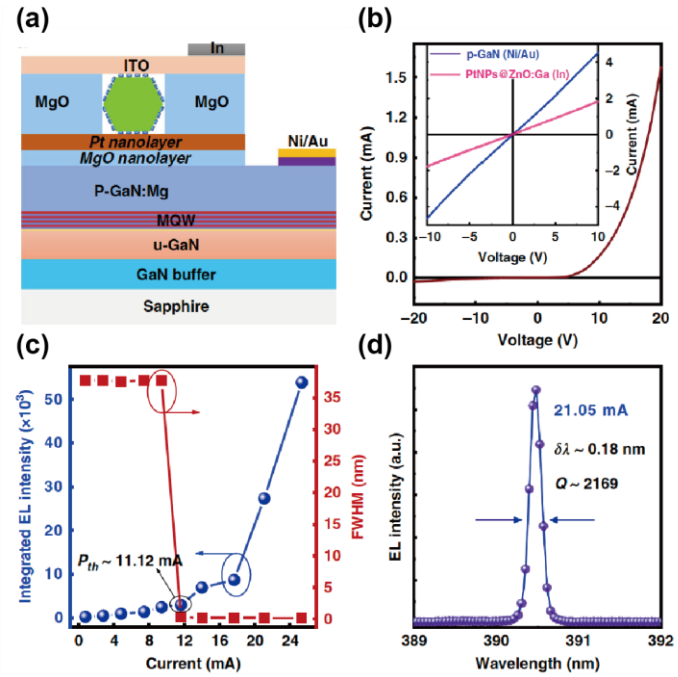

FIG. 24. (a) Schematic illustrating the cross-section of the laser device architecture based on the n-PtNPs@ZnO:Ga MW/Pt/MgO/p-GaN heterojunction. In the device configuration, ITO and Ni/Au working as electrodes are responsible for the current injection. (b) I–V curve of the fabricated single MW heterojunction emission device. Inset: the I–V curves of Ni/Au electrode contacted to the p-type GaN film, and a single PtNPs@ZnO:Ga MW, respectively. (c) Variations of the integrated EL intensity and spectral FWHM as a function of injection current, showing a lasing threshold of 11.12 mA. (d) EL spectrum via Lorentz fitting at the input current of 21.05 mA, providing the FWHM of the lasing peak $\delta\lambda \sim 0.18$ nm, and the corresponding Q-factor value is calculated to about 2169. Reproduced with permission from X. Zhou *et al.*, Light: Sci. Appl. **11**, 198 (2022). Copyright 2022 Springer Nature.

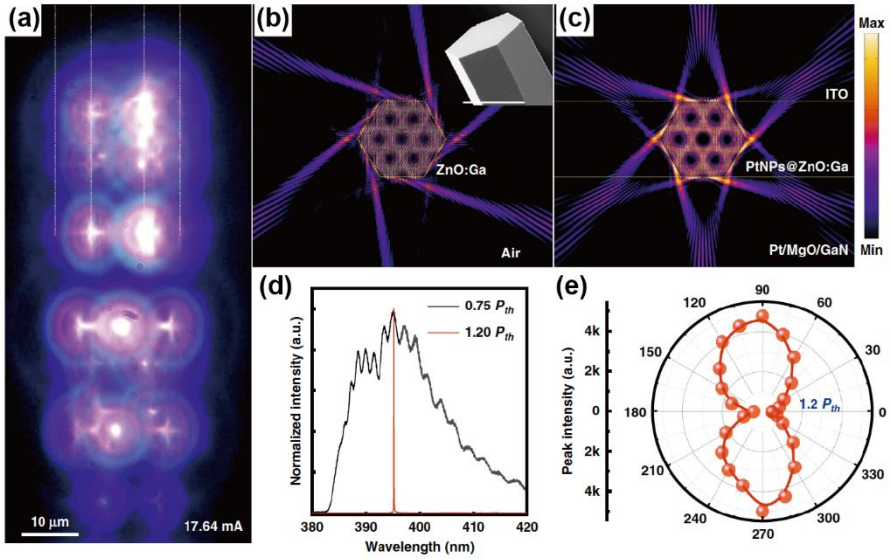

FIG. 25. (a) Optical microscopic CCD image of the emission from the fabricated device. (b) Finite-element simulations showing the standing-wave electric-field pattern of a bare ZnO:Ga wire with hexagon-shaped cross section under an optical resonant mode. Inset: SEM observation of a bare ZnO:Ga wire, that showing the hexagon-shaped cross section (Scale bar: 15 μm). (c) The simulated resonant standing-wave electric-field pattern within the cross-section of the fabricated n-PtNPs@ZnO:Ga MW/Pt/MgO/p-GaN emission device structure. (d) Normalized EL emission spectra of the fabricated device for two injection currents below (0.75 P_{th}), and above (1.20 P_{th}) the laser threshold, respectively. (e) Polarization properties of the laser emission for an operating current above the threshold (~1.20 P_{th}). The experiment EL data are symbolized by the red dots and the red solid line is the fitting result. Reproduced with permission from X. Zhou *et al.*, Light: Sci. Appl. **11**, 198 (2022). Copyright 2022 Springer Nature.

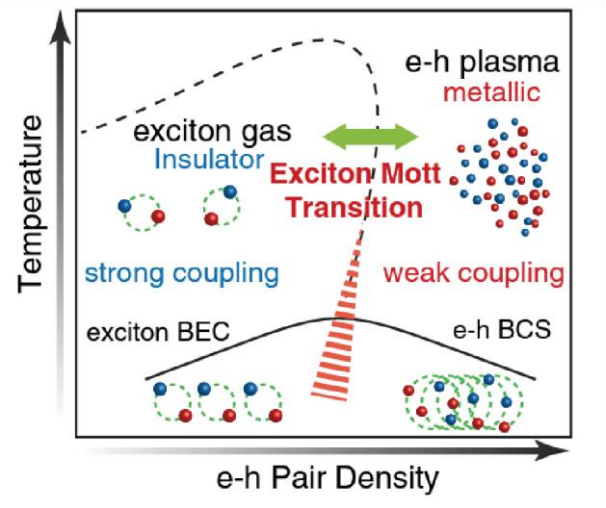

FIG. 26. Schematic phase diagram of electron-hole (*e-h*) systems in photo excited semiconductors. The theoretically anticipated quantum degenerate phases, i.e., exciton Bose Einstein condensation (BEC) and the *e-h* BCS state are also shown. Reproduced with permission from F. Sekiguchi *et al.*, Phys. Rev. Lett. **118**, 067401(2017). Copyright 2017 the American Physical Society.

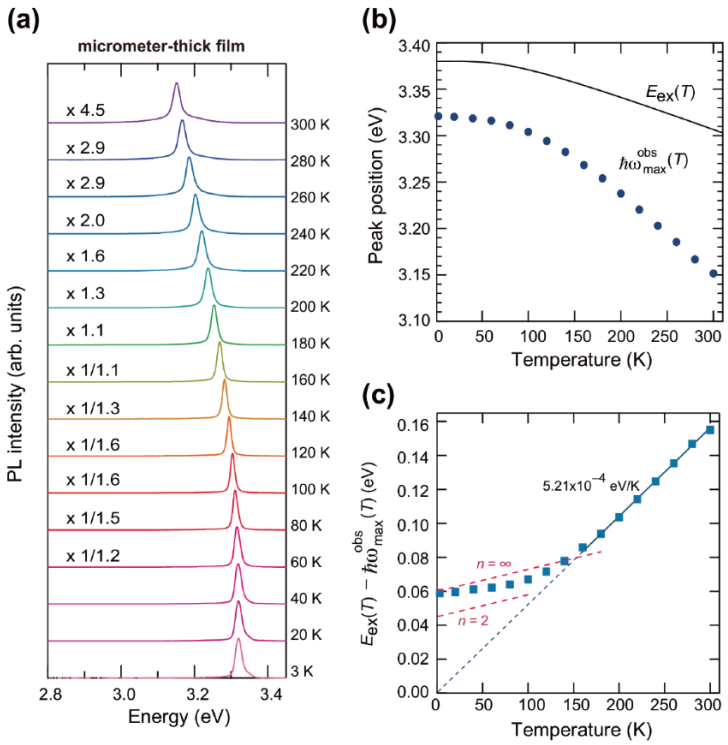

FIG. 27. Temperature dependence of the lasing spectra observed for the micrometer-sized ZnO film.(a) Changes in the lasing spectra with increasing temperature from 3 to 300K measured under a constant excitation fluence of 10.4 mJ/cm^2. The peak intensities are normalized among all spectra, which are displaced vertically for clarity. (b) The peak energy $\hbar\omega_{\mathrm{max}}^{\mathrm{obs}}$ as a function of temperature. The free-exciton transition energy E_{ex}=$E_g - E_X^b$ is also shown as a solid line. (c) The energy difference between E_{ex} and $\hbar\omega_{\mathrm{max}}^{\mathrm{obs}}$ as a function of temperature. The solid line shows a least-squares fit of the data in the temperature region from 160 to 300K to Eq. (15), which represents the temperature dependence of the emission maximum for the X-el process. The energy differences between E_{ex} and $\hbar\omega_{\mathrm{max}}^{\mathrm{X-X}}$ for n=2 and calculated from Eq. (10) are also shown as red dashed lines. One sees that the emission process changes from the X-X process to the X-el process with increasing temperature. Reproduced with permission from R. Matsuzaki *et al.*, Phys. Rev. B **96**, 125306 (2017). Copyright 2017 the American Physical Society.

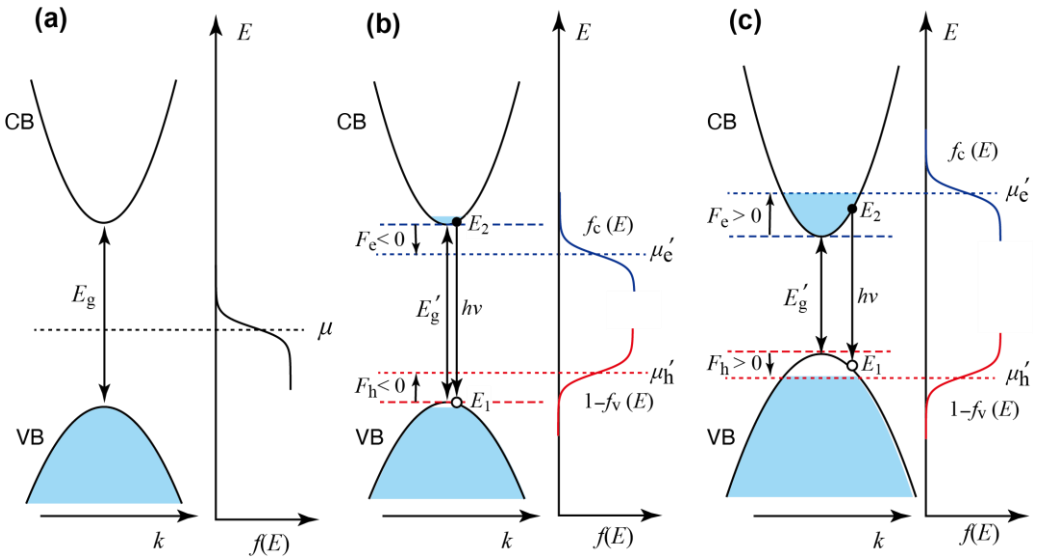

FIG. 28. Schematic representation of the conduction band (CB) and valence band (VB) symmetries near the high-symmetry Γ point with band-gap energy E_g and the corresponding Fermi-Dirac distribution function $f(E)$. The blue shaded areas indicate the states occupied largely by electrons. (a) Before photo-excitation, (b) under weak photo-excitation condition, and (c) under high photo-excitation condition. $E_g^{'}$ represents the reduced band gap, and $\mu_e^{'}$ and $\mu_h^{'}$ are the quasi-Fermi levels for electrons in CB and for holes in VB, respectively. F_e and F_h also represent the quasi-Fermi levels measured from the corresponding band extremes. $h\nu$ is the photon energy of the electron-hole recombination process indicated.

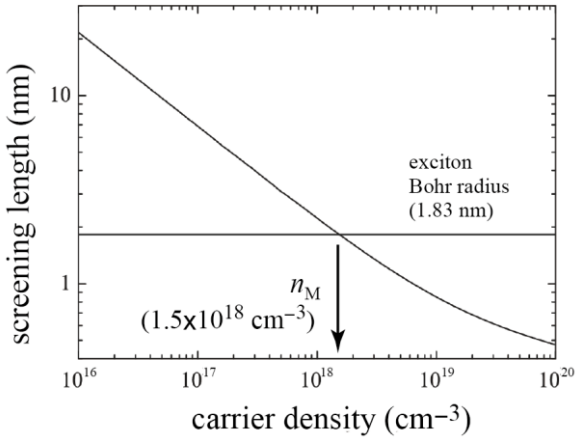

FIG. 29. Screening length at 300 K vs carrier density reported in [189]. The horizontal line indicates the exciton Bohr radius. The Mott density n_M is shown as an arrow. Reproduced with permission from M. A. M. Versteegh *et al.*, Phys. Rev. B **84**, 035207 (2011). Copyright 2011 the American Physical Society.

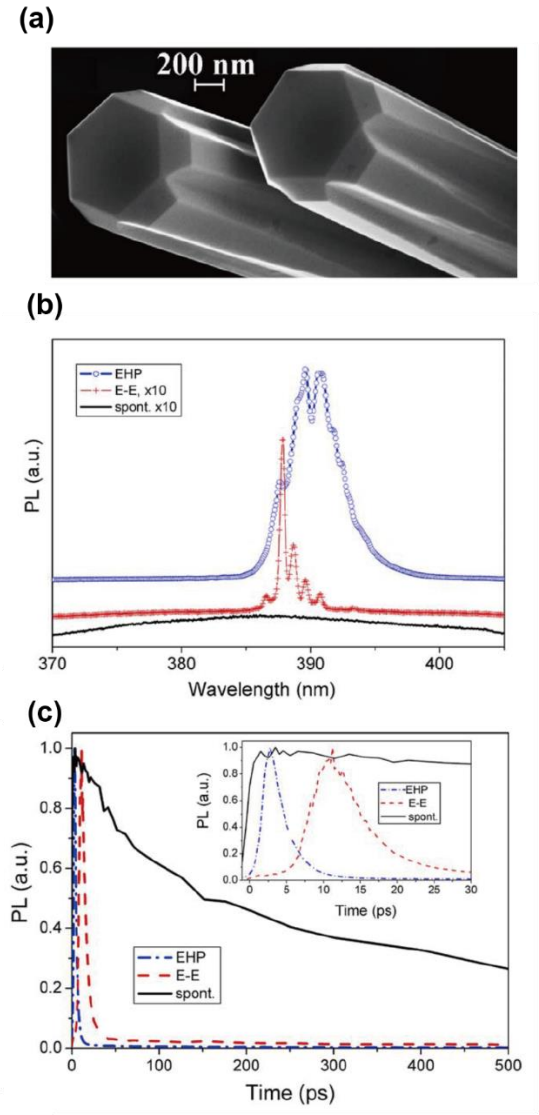

FIG. 30. (a) A representative SEM image of ZnO columns grown on Si substrates. (b) Time-resolved PL spectra for spontaneous emission (shown at 4 ps), stimulated emission due to exciton–exciton scattering (shown at 8 ps due to longer delay time), and stimulated emission due to EHP (shown at 4 ps). Due to very high intensity emission in EHP regime, the other two spectra have been multiplied by a factor 10 to improve clarity of presentation. (c) Decay curves for three different emission regimes. The inset shows enlarged region in the range from −1 to 30 ps. Reproduced with permission from W. M. Kwok *et al.*, Chem. Phys. Lett. **412**, 141 (2005). Copyright 2005 Elsevier.

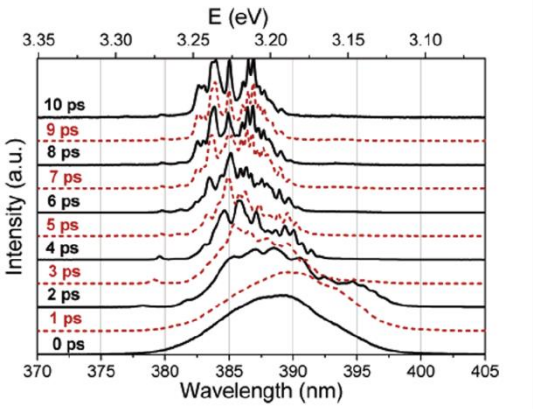

FIG. 31. Time-resolved photoluminescence from ZnO tetrapod nanowires, showing the transition from EHP to excitonic lasing regime. Reproduced with permission from A. B. Djurišić, *et al.*, J. Phys. Chem. B **109**, 41, 19228 (2005). Copyright 2005 American Chemical Socieity.